HHS Public Access

Author manuscript

Neuron. Author manuscript; available in PMC 2023 January 19.

Published in final edited form as:

Neuron. 2022 January 19; 110(2): 209–220.e6. doi:10.1016/j.neuron.2021.10.019.

Synchronized cluster firing, a distinct form of sensory neuron activation, drives spontaneous pain

Qin Zheng[1], **Wenrui Xie**[2], **Debora D. Lückemeyer**[2], **Mark Lay**[1], **Xue-Wei Wang**[3], **Xintong Dong**[1], **Nathachit Limjunyawong**[1], **Yaqing Ye**[1], **Feng-Quan Zhou**[3], **Judith A. Strong**[2], **Jun-Ming Zhang**[2,*], **Xinzhong Dong**[1,4,5,*]

[1]The Solomon H. Snyder Department of Neuroscience, Johns Hopkins University School of Medicine, Baltimore, MD, 21209, USA.

[2]Pain Research Center, Department of Anesthesiology, University of Cincinnati College of Medicine, Cincinnati, OH, 45267, USA

[3]Department of Orthopaedic Surgery, Johns Hopkins University School of Medicine, Baltimore, MD, 21209, USA.

[4]Howard Hughes Medical Institute, Johns Hopkins University School of Medicine, Baltimore, MD, 21209, USA.

[5]Lead Contact

SUMMARY

Spontaneous pain refers to pain occurring without external stimuli. It is a primary complaint in chronic pain conditions and remains difficult to treat. Moreover, the mechanisms underlying spontaneous pain remain poorly understood. Here, we employed in vivo imaging of dorsal root ganglion (DRG) neurons and discovered a distinct form of abnormal spontaneous activity following peripheral nerve injury: clusters of adjacent DRG neurons firing synchronously and sporadically. The level of cluster firing directly correlated with nerve injury induced spontaneous pain behaviors. Furthermore, we demonstrated that cluster firing is triggered by activity of sympathetic nerves, which sprout into DRG after injury, and identified norepinephrine as a key neurotransmitter mediating this unique firing. Chemogenetic and pharmacological manipulations of sympathetic activity and norepinephrine receptors suggest that they are both necessary and sufficient for DRG cluster firing and spontaneous pain behavior. Therefore, blocking sympathetic-mediated cluster firing may represent a new paradigm in treating spontaneous pain.

[*]Corresponding authors. xdong2@jhmi.edu (XZ.D.); jun-ming.zhang@uc.edu (J.-M.Z.).

AUTHOR CONTRIBUTIONS

Q.Z., W.X., D.D.L., M.L., X.W., N.L., Y.Y. performed the experiments and analyzed the data. XT.D., F. Z., interpreted the results and edited the manuscript. Q.Z. XZ.D. J.A.S. and J.-M.Z. designed the study, interpreted the results, and wrote the manuscript.

DECLARATION OF INTERESTS

No competing interests.

Graphical Abstract

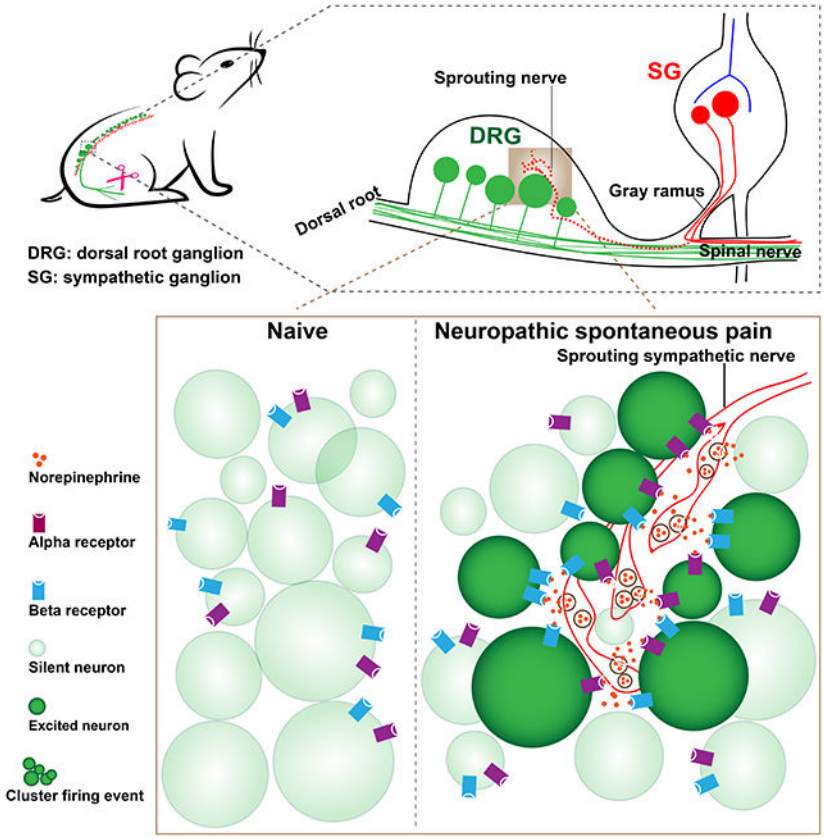

eTOC

Spontaneous pain, a primary complaint of neuropathic pain patients, is poorly understood. Zheng et al. describe a new form of sensory neuron activity: spatially clustered sensory neurons sporadically firing together, that mediates spontaneous pain in mice neuropathic pain models. Sympathetic fibers abnormally sprouting into sensory ganglia underlie this cluster firing.

INTRODUCTION

Somatosensation (e.g. touch and pain) is relayed to the spinal cord via primary sensory neurons, whose cell bodies aggregate in the dorsal root ganglia (DRG). The DRG are clusters of cell bodies comprising 10-15 thousand neurons (Schmalbruch, 1987; Sørensen et al., 2003). The central nervous system relies on primary sensory neurons to transmit sensory information in reliable spatial and temporal patterns (Prescott and Ratté, 2012). Injury to sensory nerves can alter the firing properties of DRG neurons. The result of this abnormal sensory transmission to the spinal cord is the manifestation of neuropathic pain, a condition that affects millions of people worldwide (Dahlhamer et al., 2018). Neuropathic pain can manifest as increased sensitivity to painful stimuli (hyperalgesia), pain from non-painful stimuli (allodynia), and spontaneous pain with no stimulus (ongoing pain). Spontaneous pain is the primary complaint in many neuropathic pain conditions and is found in about 96% of

neuropathic pain patients, while stimulus-evoked pain presents in less than 25% of patients (Mogil, 2012). Evoked pain has been well studied in rodent neuropathic pain models where much has been learned about the development of hyperalgesia and allodynia. However, the mechanisms involved in evoked pain are thought to differ from mechanisms causing spontaneous pain, given that drugs aimed at treating evoked pain have largely failed to treat spontaneous pain (Mogil, 2009; Murai et al., 2016). Currently, mechanisms for spontaneous pain remain poorly understood partly due to the lack of knowledge about DRG neuronal spontaneous activity at the population level, a major contributor to spontaneous pain.

Some forms of neuropathic pain are maintained by sympathetic activity both clinically and in preclinical models (Strong et al., 2018). Preclinical studies have focused on abnormal contacts between sensory and sympathetic neurons, as exemplified by early studies of sprouting of sympathetic fibers into the DRG in neuropathic pain models (McLachlan et al., 1993), studies of adrenergic hypersensitivity of sensory neurons in pain models, and more recently, by studies of sympathetic-immune interactions (Jänig, 2014). Results of preclinical studies on the role of the sympathetic system in neuropathic and inflammatory pain models have been conflicting at times, even when the same species and model are used (Strong et al., 2018). These studies have focused primarily on evoked pain behaviors, not spontaneous pain.

In this study, we utilize an in vivo calcium imaging technique developed in our lab to monitor the calcium dynamics of DRG neurons in mice with pathological pain (Kim et al., 2016). This technique allows us to visualize the activities of thousands of neurons simultaneously for hours in live animals with intact peripheral nervous system circuitry, while preserving surrounding neuronal and non-neuronal cells and circulating chemical factors. We observed a previously uncharacterized phenomenon in mice after neuropathic nerve injury, where clusters of adjacent DRG neurons fired synchronously and sporadically in groups. These events were strongly and positively correlated with the frequency of spontaneous pain behaviors. We further discovered that cluster firing of DRG neurons is provoked by activity of sympathetic nerve fibers, which were found to sprout into DRG after nerve injury. Lastly, we identify norepinephrine, released from sympathetic terminals in the DRG, as the key neurotransmitter and both α- and β- adrenoceptors expressed in DRG neurons as necessary receptors in mediating cluster firing. Together, our findings demonstrate a distinct synchronized cluster firing in DRG neurons that leads to spontaneous pain behavior and provides in vivo evidence for the ectopic “pain circuit” between sympathetic nerve fibers and sensory neurons in controlling neural-based spontaneous pain behavior.

RESULTS

Synchronized spontaneously active DRG neurons begin to cluster fire after nerve injury

Using an in vivo imaging method, we examined spontaneous neuronal activity within the DRG after spared nerve injury (SNI) of the sciatic nerve. *Pirt-Cre; GCaMP6s* mice in which a genetically-encoded Ca^{2+} indicator GCaMP6s is specifically expressed in >95% of all DRG neurons were used to simultaneously monitor the Ca^{2+} levels of ~1600 neurons from a surgically exposed DRG in live animals under anesthesia for 2 hours (Figure 1A). In mice

21 days after SNI, we observed a striking spontaneous (i.e. no external stimuli applied) pattern of Ca^{2+} signals in which neurons that were adjacent to each other sporadically fired together and formed neuronal "clusters" (Figure 1B and 1C, Movie S1). Each episode lasted many 10s of seconds and likely represented periods of multiple action potential firing (see Methods) and for simplicity are referred to here as "firing". To achieve faster imaging speed, we zoomed in to focus on a single cluster identified during the initial slow scan. We found a majority of neurons in the cluster are simultaneously active in 238 msec imaging frame (Figure S1E and S1F, Movie S2). The clustered ectopic firing of DRG neurons represents a previously uncharacterized phenomenon. It is different from the scattered singly firing neurons which we also can observe (Figure S2F). We randomly traced 15 singly firing neurons (Figure 1D) in the same imaging frames as in Figure 1C, and then calculated pairwise correlations of cluster firing neurons and singly firing neurons. We found that pairs of cluster firing neurons show significantly stronger synchrony than pairs of singly firing neurons (Figure 1E). We define a "cluster firing event" (CFE) as an observation of more than three (up to dozens of neurons, the maximum is 46 in this study) adjacently located DRG neurons that exhibit calcium transients within several continuous imaging frames. The clusters contain all sizes of DRG neurons (Figure 1F). Different clusters often fired at different times. To determine whether neurons in clusters are nociceptors, pruriceptors, low-threshold mechanoreceptors, or proprioceptors, we applied capsaicin and chloroquine onto the DRG, brushed and pinched the hind paw, and turned the ankle after imaging cluster firing events in SNI mice. We found that the neurons in the clusters contain nociceptors and low-threshold mechanoreceptors, but did not contain proprioceptors and contained very few pruriceptors (Figure S1G-S1L).

The spontaneous, non-evoked CFEs were not observed in naïve mice (Movie S3), yet slowly increased over time to 58.5% of SNI mice at post-operative day (POD) 21 (Table S1). To determine whether CFEs are induced by nerve injury, we used a second neuropathic pain model, the chronic constriction injury (CCI) of the sciatic nerve. CFEs were also observed in 52.2% mice at 14-20 days after CCI model (Table S1, Figure S1M-S1P, Movie S4), accompanied by scattered single neuron firing (Figure S2I). In SNI mice that did exhibit CFEs, we found them occurring on an average of 4 bursts per hour. Mice that displayed CFEs on average presented 2.6 clusters in the observed area of each DRG over the 2-hour imaging window. Using the CCI model, to identify the cluster neurons' peripheral targets, we injected CTB 555 into skin and muscle separately in different mice, and found that the neurons in the clusters innervate both skin and muscle (Figure S1M and S1N).

We next examined whether CFEs were specific to neuropathic pain from nerve injury. To test this, we carried out in vivo imaging in several other pain models including an inflammatory pain and a bone cancer pain model. No CFEs were observed in the complete Freund's adjuvant (CFA) or the formalin inflammatory pain models (Table S1). In the bone cancer pain model, CFEs were only observed in 1 out of 10 mice examined (Table S1). While we saw increased scattered singly firing DRG neurons in mice across all injury types, CFEs were consistently observed only in neuropathic pain models (Figure S2A-S2I). After quantifying the numbers of singly firing neurons in various pain models, we found that the singly firing neurons occurred at higher frequency (Figure S2J) than in naïve mice.

Interestingly, a CFE is distinct from the coupled firing observed in our previous study (Kim et al., 2016) that was observed only after stimuli applied to the paw in the both neuropathic and inflammatory pain models, and that was dependent on gap junctions in neurons and satellite glia. A CFE is also different from propagating intercellular calcium waves in neurons caused via gap junctions in the central nervous system (Charles et al., 1996; Kuchibhotla et al., 2009; Wilkins and Sneyd, 1998). We found that neither CFEs nor singly firing neurons could be blocked by the gap junction inhibitor, carbenoxolone (CBX 50μM) (Figure S3A-S3F). CFEs are also uncoupled from satellite glia activity (Figure S3G and S3H). Strikingly, topical administration of lidocaine to sciatic nerve injury sites blocked singly firing events but not cluster firing events whereas topical application of lidocaine onto the DRG blocked all firing (Figure S3I-S3N). These data suggest that cluster firing events occur mainly in the ganglion and singly firing events are mainly triggered by peripheral activation.

Collectively, our data indicate that these previously uncharacterized cluster firing events are specifically associated with nerve injury.

Spontaneous pain behaviors directly correlate with CFE

To investigate whether spontaneous pain behaviors are correlated with higher frequencies of CFEs, we first examined the spontaneous behavior in naïve and SNI mice 21 days after surgery. The number of bouts of spontaneous licking and flinching/shaking/lifting of the ipsilateral hind paw was recorded by a scorer blinded to the cluster firing phenotype. Mice were imaged for spontaneous cluster firing in the L4 DRG immediately after behavioral filming. We found that SNI mice exhibiting cluster firing had much higher spontaneous pain scores than naïve mice or SNI-treated mice that did not show cluster firing (Figure 1G). This suggested that the ectopic spontaneous cluster firing may correlate with the observed intermittent spontaneous pain behaviors. We further quantified the frequency of spontaneous pain behaviors and occurrence of CFEs of the same animal during the in vivo imaging session on the same day. Overall, we found a significant positive correlation between spontaneous pain behaviors and the frequency of CFEs (Figure 1H) and total duration of CFEs (Figure S1Q). Surprisingly, we did not find a significant difference in evoked mechanical pain between SNI mice with and without CFEs evaluated the day before we carried out in vivo imaging. (Figure 1I and 1J). Together, these data suggest that CFEs may contribute to spontaneous pain but not evoked mechanical pain.

Anatomical loci of CFE correspond to targets of sprouted sympathetic fibers after nerve injury.

In addition to finding that administration of lidocaine to sciatic nerve injury sites blocked singly firing events but not cluster firing events, we also observed that CFEs did not occur at random locations. When diagrammed, they seemed to occur at the border, preferentially near the poles of the DRG (Figure 1K). This spatial specificity reminded us of an observation reported in 1993 that sympathetic nerves sprouted into the DRG after nerve injury at very similar locations (McLachlan et al., 1993). This location of sprouted fibers at DRG borders was confirmed in our own microscopy data (see below). However, there has been no study directly demonstrating the functional significance of the sympathetic innervation

with regards to CFEs and pain. Moreover, in this previous study, they used anti-tyrosine hydroxylase (TH) staining for sympathetic fibers in the DRG, and it is now known that a small population of DRG neurons are TH-positive in normal animals (Brumovsky et al., 2006). Hence, to investigate whether the locations of the CFEs correspond to anatomical locations of sympathetic sprouting, we used a sympathetic specific *Phox2b-Cre* mouse line (Huber, 2006; Pattyn et al., 1999; Zeisel et al., 2018) (Figure S3O) instead of relying only on the TH staining technique and generated *Phox2b-Cre;Rosa26-LSL-tdTomato (tDT); Pirt-GFP* mice (Figure 2A), and examined whether tDT signal could be detected directly in DRG after SNI. Following SNI in the transgenic mice, DRGs were dissected and treated according to a clearing protocol as previously described (Susaki et al., 2014). We compared clearing-derived images of naïve and SNI mice and found abundant sympathetic fibers in SNI mice but not the naïve animals (Figure 2B-2D). This increase in the density of sympathetic fiber not colocalized with blood vessels after SNI was quantitatively confirmed using immunohistochemical methods in DRG sections (Figure S3P and S3Q) and confirmed using traditional anti-TH staining (Figure S3R and S3S), and was blocked by localized sympathectomy (data not shown). As in our previous study in rat (Xie et al., 2020) SNI model, we primarily observed increased fiber density rather than the “basket” formations seen in some other pain models. In a different mouse model in which both excess fibers and basket formations are observed, we observed that both were associated with increased excitability of nearby neurons (Xie et al., 2011).

We next performed retrograde tracing from the DRG to the sympathetic ganglia by injecting CTB555 into DRGs in naïve and SNI mice. Enhanced CTB signal in the adjacent sympathetic ganglia of mice with SNI injury was observed (Figure 2E-2G). A relatively small number of sympathetic neurons were labeled, and this number increased significantly after SNI (Figure 2H). In addition, we performed SNI surgery on *Phox2bCretdT* mice and injected GCaMP6 virus to infect DRG neurons (Figure S4A), to simultaneously detect sprouted sympathetic fibers and CFEs in vivo. We found that not all SNI mice show sprouting in the DRG, and the cluster firing only occurred in mice with sympathetic sprouting (Table S2). In addition, the cluster firing sites colocalized with sites of sympathetic nerve sprouting (Figure S4B-S4C). Together, these data demonstrate that sympathetic nerve fibers abundantly extend into DRG after nerve injury and the location of sympathetic innervation reflected the location of the CFEs.

Inhibition of ectopic sympathetic nerves attenuates CFEs and spontaneous pain.

To directly test whether sympathetic innervation contributed to spontaneous CFEs and pain, we first examined whether temporary pharmacological blockade of sympathetic nerve fibers in the DRG could affect spontaneous cluster firing. 6-OHDA is commonly used to inhibit the neurotransmitter release of sympathetic nerves (Mazzuca and Poulain, 1974). Treating the DRG with 6-OHDA did not reduce singly firing neurons (Figure S4F), but significantly reduced the incidence of CFEs (Figure 3A-3G), including the total number of clusters (Figure 3E), frequency of cluster firings (Figure 3F), and total number of cluster firing neurons (Figure 3G). However, no inhibition of cluster firing was observed with addition of vehicle (saline) (Figure 3E-3G, Figure S4D-4E). These data showed that acute blockade of sympathetic nerve terminals, which sprout into DRG after nerve injury, can reduce the

incidence of CFEs. We also found that spontaneous pain scores significantly decreased after i.t. administration of 6-OHDA versus vehicle in SNI mice (Figure S4I), although higher doses led to deleterious effects most likely spinally mediated. To avoid possible confounds of spinal effects of i.t. injections, we next crossed *Phox2b-Cre* mice with *Gi-DREADD* mice to investigate whether specific chemogenetic silencing of sympathetic activity after nerve injury could decrease the spontaneous cluster firing as was observed with pharmacological inhibition. For these experiments, we used AAV9.CAG.GCaMP6s to infect and visualize lumbar DRG Ca^{2+} activity at POD 7 in SNI mice (Figure 4A and 4B). On POD 21, we found that acutely inhibiting sympathetic activity by topical application of CNO but not vehicle diminished the incidence of CFEs (Figure 4C-4G, Figure S5A and S5B), though not singly firing neurons (Figure S5C).

To investigate whether the reduction of spontaneous cluster firing in DRG can affect spontaneous pain behavior, we then examined the spontaneous pain scores before and after i.t. administration of CNO in mice presenting with cluster firing. Mouse behavior was videotaped 1 hour before and 1 hour after the i.t. injection of CNO. In vivo imaging was performed the next day to record spontaneous cluster firing. We found that spontaneous pain scores significantly decreased after i.t. administration of CNO versus vehicle in SNI mice with cluster firing (Figure 4H). Strikingly, spontaneous pain scores are not affected by i.t. administration of CNO in SNI mice without cluster firing (Figure S5E). Collectively, these results show that chemogenetic silencing of sympathetic nerves, which sprout into the DRG after nerve injury, diminishes the incidence of CFEs and relieves spontaneous pain.

As additional evidence for the role of local sympathetic fibers in spontaneous pain behaviors and cluster firing, we performed a very localized “microsympathectomy” (mSYMPX) at the time of SNI. This procedure consisted of cutting the grey rami (postganglionic sympathetic fibers) near their juncture with the spinal nerves near the L3 and L4 DRGs (Tonello et al., 2020). As shown in figure S4J, the spontaneous pain score increased gradually after SNI (compare to the gradual increase in number of mice with cluster firing from Table S1); mSYMPX reduced the spontaneous pain score at later time points. We also examined the effect of mSYMPX on cluster firing. As these experiments were done with a different in vivo imaging system, we first confirmed the existence of cluster firing 3-5 weeks after SNI (Figure 3H-3I, Movie S5). In these experiments 5 out of 8 (62.5%) of mice exhibited cluster firing, a percentage quite similar to that observed in Table S1 at day 21 (58%). This cluster firing was greatly reduced by the mSYMPX procedure. In recordings before and immediately after acute mSYMPX in the same animal, no cluster firing events could be observed after the mSYMPX procedure (Figure 3J). mSYMPX performed at the time of SNI, or performed 7 days prior to the in vivo recording, also reduced the incidence of cluster firing (Figure 3J).

Activation of ectopic sympathetic nerves enhances incidence of CFEs and spontaneous pain

Our previous experiments examined effects of loss of function of sprouted sympathetic activity on the incidence of cluster firing and spontaneous pain behaviors. We next examined the effect of gain of function on sympathetic activity. To selectively activate

sympathetic activity in vivo, we bred *Phox2b-Cre* mice with *Gq-DREADD* mice. Again, AAV9.CAG.GCaMP6s was used to infect and visualize lumbar DRG neurons at POD7 after SNI (Figure 5A and 5B). On POD21, we found that acutely activating sympathetic fibers by topical application of CNO enhanced the incidence of CFEs in the DRG (Figure 5C-5G), versus vehicle application (Figure S5F and S5G, Figure 5E-5G). Interestingly, singly firing neurons were not affected (Figure S5H). Similarly, we found that spontaneous pain scores were significantly increased after i.t. administration of CNO in mice with cluster firing, when compared to vehicle administration (Figure 5H). However, spontaneous pain scores did not change after i.t. administration of CNO in SNI mice without cluster firing (Figure S5J). Taken together, these results show that chemogenetic activation of sympathetic activity in the DRG with nerve injury, enhances the incidence of CFEs and spontaneous pain.

We also examined whether CNO can affect the incidence of cluster firing and spontaneous pain behavior in *Phox2b-Cre* mice not expressing the DREADD receptor (Figure S5K-S5Q). Importantly, no change was observed, further supporting the finding that increases (or decreases) in the incidence of cluster firing and spontaneous pain behavior are the specific result of chemogenetic activation (or inhibition) of sympathetic fibers innervating the DRG.

In summary, using different approaches for directly manipulating sympathetic activity, we demonstrated that spontaneous cluster firing of DRG neurons after peripheral nerve injury was sympathetic-mediated, and that cluster firing contributed to spontaneous pain.

SNI evokes endogenous NE release in DRG

We next sought to elucidate the molecular mechanisms by which sympathetic activity triggers and drives CFEs. We first examined a primary neurotransmitter known to be released by sympathetic nerve endings. Earlier studies have shown that most postganglionic sympathetic nerves, including those in the lumbar ganglia, release the transmitter norepinephrine (NE) (McCorry, 2007). To specifically determine if the sprouted sympathetic nerve fibers in the L4 DRG release NE, we used an adeno-associated virus (AAV) to express a genetically encoded GPCR activation-based norepinephrine (GRAB NE) sensor in DRGs in WT mice after SNI (Figure 6A). The sensor is capable of displaying a large increase in fluorescence in the presence of extracellular NE, allowing for spatially and temporally precise measurement of localized NE release (Feng et al., 2019). We validated that the sensor expressed robustly in the DRG neurons and specifically responded to NE (Figure S6G, Figure 6C). We found that endogenous NE release was only observed in the SNI mice but not in the naïve mice (Figure 6C-6G). Strikingly, the NE release was also observed in clusters of sensory neurons. The decay time of the sensor was very slow, precluding observation of repeated NE release events or calculation of their frequency. To examine the potential involvement of dopamine (another neurotransmitter released by sympathetic nerves) in cluster firing, we also used a similarly-designed dopamine sensor (Sun et al., 2018) and detected no dopamine release in the DRG after nerve injury (Figure S6A-S6F). These data show that following nerve injury, NE was released by ectopic sympathetic nerve fibers in the DRG with a spatial pattern similar to that of cluster firing.

In addition, we applied both low and high concentrations of NE (50 μM and 500 μM) on DRGs from naïve or SNI mice with and without cluster firing. Compared to naïve DRG and

injured DRG without cluster firing, injured DRG with cluster firing showed a much more robust response (Figure S6H-S6J). These results are consistent with numerous previous studies on adrenergic hypersensitivity of sensory neurons after nerve injury and suggest the phenomenon is especially observed in cluster firing neurons. As in a previous study (Uttam et al., 2018) this hypersensitivity was not attributable to increases in adrenoceptor mRNA expression in the DRG after SNI (Figure S7E); instead, alternative mechanisms may include changes in membrane trafficking or posttranslational modifications of adrenoceptors. In addition, we found the most neurons in the clusters responded to 500 μM NE (Figure S6K). The percentage of neurons in the clusters responding to 500 μM NE was 71.51% ± 7.97 (N=5 clusters in 3 SNI mice with clusters, Figure S6L).

Local blockade of adrenergic receptors in DRGs suppresses CFEs and relieves spontaneous pain

We then attempted to pharmacologically block NE receptors in DRG and examine the effect on CFEs and spontaneous pain. Both α- and β-adrenoceptors are expressed in DRG neurons (see Discussion). We found that both phentolamine (non-selective α blocker) and propranolol (non-selective β blocker) significantly reduced the incidence of CFEs and spontaneous pain (Figure 7), when compared to vehicle (saline) (Figure 7, Figure 3E-3G, Figure S4D-S4F). Neither antagonist inhibited singly firing neurons (Figure S7A). We confirmed that both α- and β- adrenoceptors were expressed in the mouse DRG after SNI using quantitative reverse transcription PCR (Figure S7E). Expression of presynaptic inhibitory α2 adrenoceptors in sympathetic postganglionic nerve has been observed previously (Gyires et al., 2009), though they may also be expressed in sensory neurons where they can have excitatory or pronociceptive effects, especially after injury (Cho et al., 1997; Ma et al., 2005). We applied antagonists of α1 and α2 receptors on DRGs in SNI mice with clusters. We found α1 antagonists could inhibit CFEs, but α2 antagonists could not (Figure S7F-S7U). Neither antagonist could inhibit singly firing neurons (Figure S7K, S7S). Collectively, these results suggest that noradrenergic signaling within DRG neurons after nerve injury is necessary for CFEs and spontaneous pain.

DISCUSSION

DRG neurons are the primary sensory neurons within the somatosensory pathway, receiving multiple types of information that is relayed to the spinal cord. Previous studies have reported that abnormal spontaneous activity in individual sensory neurons is a common feature of many pain models and is a likely candidate for mediating spontaneous pain (Benzon et al., 2011; Kajander et al., 1992; Zheng et al., 2012). However, all the available information is from studies on cultured or isolated ganglia, where the activity of individual neurons was recorded. With the recent advances in technology such as in vivo calcium imaging, investigators were able to observe large populations of DRG neurons simultaneously (Chisholm et al., 2018; Emery et al., 2016; Wang et al., 2018). Nevertheless, population level data of spontaneous activity exhibited by DRG neurons under pathological conditions from intact animals have not been studied.

Here, we discovered two different types of spontaneous activity in the DRG including the previously undescribed spontaneous cluster firing that is specifically associated with peripheral nerve injury. More importantly, we found that clusters of synchronized firing in the DRG drive spontaneous pain in mice with nerve injury. This phenomenon represents a novel form of DRG neuronal activation and provides a conceptual advance that broadens our understanding of spontaneous activity and its relation to spontaneous pain. We also observed single-neuron firing that is common in all of the pain models used in the current study, and is consistent with the previous studies in which single neurons were recorded. While such single neuron firing and other mechanisms likely make some contribution to spontaneous pain (as some increase in spontaneous pain is observed even in mice without cluster firing, and very early spontaneous pain is not reduced by sympathectomy), much more spontaneous pain is observed in mice with cluster firing. It is likely that previous studies failed to observe cluster firing because it requires simultaneous detection of activity in multiple neurons, which was only recently feasible, and because its intermittent nature makes it harder to detect with short term electrical recording. Interestingly, we found these two types of activity could be differentially regulated.

Early studies first made observations pointing to sympathetic innervations in the DRG after nerve injury (McLachlan et al., 1993). However, in the last few decades, no study has directly demonstrated the functional significance of this sprouting with regards to spontaneous pain. Furthermore, no study has shown how sympathetic nerves can evoke DRG neuron activation in vivo (i.e. neurotransmitters and receptors) again due to the lack of molecular and in vivo imaging tools. To answer this gap in knowledge we used chemogenetic techniques to specifically manipulate sympathetic nerves while employing in vivo imaging and biosensors to finally resolve what had previously been only a loose understanding of post-injury sprouting. We identified that the CFE phenomenon is caused by ectopic sympathetic nerve activity in the DRG, and is both necessary and sufficient to trigger spontaneous pain behaviors after nerve injury.

Our study provides evidence that sympathetic sprouting in the DRG plays a role in spontaneous pain in the SNI and related neuropathic pain models. This expands our knowledge from some previous studies showing sympathetic dependence of evoked pain in rat (Xie et al., 2020), although this has been somewhat controversial (Han et al., 2006; Pertin et al., 2007). As discussed in our previous study (Xie et al., 2020), there is also disagreement between labs in the degree and timing of sympathetic sprouting in the DRG in the SNI model, perhaps reflecting differences in animal stress, husbandry practices, or unknown variables, and perhaps modeling the variability in human patients. Here we observed that interanimal variability in sprouting correlated with variability in spontaneous pain. It will be important to revisit the question of sympathetic dependence of pain in preclinical models focusing on spontaneous pain. Our findings are also of interest in view of clinical studies of chronic pain patients that show increased spontaneous pain may result from sympathetic activation or stress, as well as studies that show adrenergic hypersensitivity in human pain patients (Baron, 2009; Light et al., 2009; Walters, 2018).

We provided direct evidence that spontaneous intermittent NE release in the DRG was related to cluster firing, although differences in the response characteristics of the NE and

Ca^{2+} sensors preclude a direct comparison of the frequency and duration of these events. Our study also showed that locally blocking either α or β receptors at the level of the DRG reduced cluster firing. Interestingly, we found the inhibiting α1, but not α2 receptors can inhibit CFEs. This is consistent with some previous studies showing excitatory effects of α1 or β receptor stimulation on rodent DRG neurons, especially after nerve injury (e.g., (Maruo et al., 2006) (α1), (Du et al., 2019) (β2). However, systemic effects of adrenergic antagonists would likely be more complex due to the presence of the receptors in spinal cord and brain, where they in some cases play an anti-nociceptive role, and there are some disagreements in the preclinical literature about the role of specific receptor subtypes. Further studies will be needed to dissect out the possible contributions of adrenoceptors expressed on sympathetic fibers (Furlan et al., 2016; Sapio et al., 2020) in the DRG after nerve injury.

Spontaneous pain may be either ongoing or paroxysmal (Bennett, 2012). Ongoing pain is often described as burning pain, and is thought based on human and animal studies to be dependent on small size C fibers (Djouhri et al., 2006; Odem et al., 2018). Paroxysmal pain is described as shooting pain or electric shock-like, and is thought to depend on large size Aβ fibers (Devor, 2009; Truini et al., 2008, 2009). Nerve injury can also cause a phenotype switch where nociceptive transmitters and spontaneous activity are seen in medium-to large diameter A-type DRG cells. Interestingly, we observed neurons of all sizes in the firing clusters. Furthermore, one decades old clinical observation has shown that sympathetic sprouting is observed in DRGs removed from human neuropathic pain patients (Shinder et al., 1999). Thus, the cluster firing phenomenon we present here would most likely be related to both intermittent paroxysmal pain and the maintenance of ongoing pain in humans. Future studies will be required to better understand what types of neurons are in the clusters and what their roles are in transmitting pain signals. A spatial pattern of cluster firing at the population level is distinct from temporally patterned spiking at the single neuron level. We observed, however, that nerve injury-induced sympathetic sprouting caused large populations of neurons of all sizes to fire synchronously in the DRG without any sensory stimuli. This phenomenon could potentially represent a severe pathology in which the CFEs disturb the proper relay of sensory information and cause alterations in spinal processing, versus those signals relayed from a single sensory neuron. Thus, clusters of neurons firing in the DRG may have a unique role in processing and triggering spontaneous pain, similar to the synchronous neuronal firing that occurs in clusters of microdomains at onset of seizures. Based on the previously unrecognized role of sympathetic signaling pathways in triggering cluster firing and spontaneous pain, manipulating these neurons and pathways could be a therapeutic target for spontaneous pain.

STAR METHODS

RESOURCE AVAILABILITY

Lead contact—Further information and requests for resources and reagents should be directed to and will be fulfilled by the lead contact, Xinzhong Dong, xdong2@jhmi.edu

Materials availability—This study did not generate new unique reagents.

Data and code availability

- All data reported in this paper will be shared by the lead contact upon request..
- This paper does not report original code.
- Any additional information required to reanalyze the data reported in this paper is available from the lead contact upon request.

EXPERIMENTAL MODEL AND SUBJECT DETAILS

Ethic statement—IACUC Institutional Review Boards at the Johns Hopkins University School of Medicine and University of Cincinnati approved all animal procedures. Experiments were conducted in accordance with the National Institute of Health Guide for the Care and Use of Laboratory Animals.

Mouse strains—C57BL/6 mice were purchased from Jackson (Jax) Laboratories. *Pirt-cre* mice were generated as previously described via homologous recombination (Kim et al., 2016). *Rosa26-lox-stop-lox GCaMP6s* mice were acquired from Dr. Bergles' Lab at Johns Hopkins. *Pirt-Cre; GCaMP6s* mice were obtained by crossing *Pirt-Cre* mice with *Rosa26-lox-stop-lox GCaMP6s* animals. *Pirt-GCaMP3 (GFP)* mice were generated and described in a previous study (Kim et al., 2008, 2016). *Phox2b-Cre, GFAP-Cre,* Ai14 strain B6.*Rosa26-stop (flox) -tdTomato*, *Rosa26-LSL-Gq-DREADD* and *Rosa26-LSL-Gi-DREADD* mice were purchased from Jax Laboratories. All transgenic mice used in all animal experiments were heterozygous, unless otherwise indicated. The mice were 2–3-month-old from both sexes that had been backcrossed to C57BL/6 mice for at least five generations. The day before the behavioral tests, all mice were acclimated for at least 30 min to their testing environment. We housed 4-5 mice in each cage in the vivarium with 12h light/dark cycle (Johns Hopkins University) or 14h light/10 h dark (Univ. of Cincinnati) and all the behavioral tests were performed in the morning.

METHOD DETAILS

Mouse models and microsympathectomy—To generate the SNI nerve injury model, we anesthetized mice with 1.5%–2% isoflurane using a gas vaporizer. After skin and muscle incision, 2 of the 3 terminal branches of the sciatic nerve (SN) were tightly ligated with 8-0 silk suture, sparing the tibial nerve or sparing the sural nerve. Then, the ligated branches were transected distal to the ligature, and around 2 mm of each distal nerve stump was cut. The incision was closed with sutures or tissue glue.

To generate the sciatic nerve CCI nerve injury model, we anesthetized mice with 1.5%–2% isoflurane gas using a gas vaporizer. SN was exposed at the level of the mid-thigh by a small dissection, and the nerve was isolated from surrounding tissues. The chronic constriction injury was performed with loosely ligated with 9-0 silk sutures around the unilateral SN. The incision was closed with sutures or tissue glue. Imaging and behavioral experiments and were performed at different time points after the SNI or CCI surgery, as indicated.

To generate the Formalin model, we injected 10 μL formalin (2% in saline) into the hindpaw. Then imaging experiments were performed immediately.

To generate the CFA inflammatory model, we mixed CFA and saline in a 1:1 ratio and injected them (10 μL) subcutaneously into glabrous skin of the hindpaw. Two or three days later, imaging experiments were performed.

To generate the B16F10 tibial bone cancer model, we cultured B16F10 melanoma cells (ATCC) in Dulbecco's modified Eagle's medium (DMEM) enriched with 10% fetal calf serum (Gibco). Then we collected and injected a suspension of 10^5 cells in a volume of 5 μL of PBS into the intramedullary canal of the tibia bone of mice anesthetized with 1.5%–2% isoflurane gas. The wound was closed with a surgical suture. 14 days later, imaging experiments were performed. “microsympathectomy” (“mSYMPX”) was performed as originally described in rats (Xie et al., 2016) and adapted for mice (Tonello et al., 2020). Briefly, the proximal L3 and L4 spinal nerves and transverse processes on one side were exposed. The spinal nerves (ventral rami) were visualized and freed from surrounding tissue. The gray rami entering the L3 and L4 spinal nerves close to the DRG were identified on the ventral side of the spinal nerve close to the intervertebral foramen. At this site, where the gray ramus merges into the spinal nerve, the gray rami and nearby connective tissue were gently dissected away from the nearby blood vessels and cut and disconnected from spinal nerve. Approximately 1 mm of gray ramus was further removed to make a gap and slow regeneration. Both L3 and L4 gray rami were cut. Sham controls received similar exposure of the spinal nerves, but the gray rami were not cut. These surgeries were performed during the same surgery as that implementing the SNI model except where indicated.

Withdrawal threshold to mechanical stimulation—To assess mechanical allodynia, naïve and SNI mice at day 20 after surgery were placed in a closed plexiglass chamber with a mesh floor through which stimulus probes could be applied. After a period of acclimation, calibrated Von Frey filaments (0.07 and 0.4 g) were applied to the ipsilateral hind paw for approximately 1 s. Each stimulation was repeated 10 times, and paw withdrawal frequency was determined as described previously (Guan et al., 2010).

Spontaneous pain behavior observation—To examine spontaneous pain behavior, animals were placed in individual plexiglass containers and videotaped for 60 minutes. The video recording was subsequently played back in slow motion and the number of bouts of licking and flinching/shaking/lifting with the ipsilateral hind paw was counted. Movements associated with exploratory behavior, locomotion, body repositioning, and grooming were excluded. One bout of licking was counted as 2 points, and one bout of flinching/shaking/lifting was counted as 1 point, and the total number of points for the 1-hour recording was used as the spontaneous pain score (Dubuisson and Dennis, 1977; Jourdan et al., 1997).

DRG exposure surgery for in vivo imaging—For all imaging experiments, mice 2 months or older were anesthetized by i.p. injection of sodium pentobarbital (40–50 mg/kg). After deep anesthesia was reached, the animal’s back was shaved and aseptically prepared, and ophthalmic ointment (Lacrilube; Allergen Pharmaceuticals) was applied to the eyes to prevent drying. During the surgery, mice were kept on a heating pad (DC temperature controller, FHC) to maintain the body temperature at 37°C ± 0.5°C as monitored by a rectal probe.

Dorsal laminectomy over the DRG was performed, usually at spinal level L6 to S1 below the lumbar enlargement (but occasionally below S1) but without removing the dura. Some experimental conditions, such as direct local drug administration into DRG tissue, required the removal of the dura. A 2-cm-long midline incision was made around the lower part of the lumbar enlargement area; next, 0.1 mL of 1% lidocaine was injected into the paravertebral muscles, and these were dissected away to expose the lower lumbar part which surrounds the L3–L5 vertebra bones. The L4 DRG transverse processes were exposed and cleaned. Using small rongeur, we removed the surface aspect of the L4 DRG transverse process near the vertebra (only the L4 DRG transverse process was removed, but the bone over the spinal cord was intact) to expose the underlying DRG without damaging the DRG and spinal cord. Bleeding from the bone was stopped using styptic cotton.

In vivo DRG calcium imaging—In vivo imaging of whole L4 DRG in live mice was performed for 2–7 hr immediately after the exposure surgery. Body temperature was maintained at 37°C ± 0.5°C on a heating pad and rectal temperature was monitored. After exposure surgery, mice were laid down in the abdomen-down position on a custom-designed microscope stage. The spinal column was stabilized using custom-designed clamps to minimize movements caused by breathing and heart beats. In addition, a custom-designed head holder was also used as an anesthesia/gas mask. The animals were maintained under continuous anesthesia for the duration of the imaging experiment with 1%–2% isoflurane gas using a gas vaporizer. Pure oxygen was used to deliver the gas to the animal.

The microscope stage was fixed under a laser-scanning confocal microscope (Leica LSI microscope system), which was equipped with macro-based, large-objective, and fast EM-CCD camera. Live images were acquired at typically ten frames with 600 Hz in frame-scan mode per 7 s, at depths below the dura ranging from 0 to 70 μm, using a 5× 0.5 NA macro dry objective at typically 512 × 512 pixel resolution with solid diode lasers (Leica) tuned at excitation 488 nm wavelength and emission at 500–549 nm for green fluorescence. For zoomed-in faster scanning, it takes 0.238 s/frame to image individual ensembles of cluster firing (256x256 pixel). For analysis, raw image stacks (512 × 512 pixels in the x–y plane and 10–30 αm voxel depth; typically 10 optical sections) or raw zoomed-in faster scanning imaging frame (256x256 pixels in one frame, one section) were imported into ImageJ (NIH) for further analysis. DRG neurons were at the focal plane, and imaging was monitored during the spontaneous activation of DRG neuron cell bodies without peripheral stimuli. The imaging parameters were chosen to allow repeated imaging of the same cell for a long time without causing damage to the imaged cells or to surrounding tissue. At the end of each experiment, the viability of the DRG was confirmed by observing large numbers of cells giving a calcium transient in response to pinching of the hindpaw (Figure S1G-S1H, Figure S4G-S4H, Figure S5D and S5I, Figure S7B-S7D, S7L-S7M, S7T-S7U). GCaMP6s was chosen as a highly sensitive calcium indicator with slow kinetics. It is capable of detecting single action potentials in vivo under optimized recording conditions. However, under more typical in vivo recording conditions (especially, lower magnification as used here), detection of single action potentials is less reliable, but the dye instead gives a single integrated single waveform in response to action potentials separated by an interval on the order of 100-150 ms or less (Chen et al., 2013; Huang et al., 2021). Hence, in sensory neurons that

when spontaneously active generally have much higher firing frequencies, it is likely that the observed calcium transients (referred to here as "firing") represent integrated signals of multiple action potentials and that cells firing only one or a few action potentials would not have been detected. We confirmed that GCaMP6s behaved in this fashion when expressed in DRG cells using an ex vivo preparation with simultaneous intracellular microelectrode recording (supplemental figure S1A); decay half time constants were on the order of 1 – 3 seconds, consistent with previous reports in other types of neurons. In some experiments we also use lidocaine to determine neuronal excitability. We recorded the activated neurons by brushing and pinching the hind paw before (1st) and after (2nd) application of 1.5% lidocaine onto the DRG. We found that lidocaine can totally inhibit all neurons' activation by brushing and pinching. 3 hours after washing out lidocaine, we brushed and pinched again (3rd), we found that the neurons recovered (Figure S1B-S1D).

In vivo calcium imaging data analysis—For imaging data analysis, raw image stacks were collected, and imported into FIJI (NIH) for further analysis. Optical planes from sequential time points were first re-aligned and motion corrected using a cross-correlation-based image alignment plugin in FIJI software to compensate for minor motion shifts during the acquisition. The contrast was adjusted, and selected optical planes or z projections of sequential optical sections were used to obtain final images and to produce time-lapse movies. Calcium signal amplitudes were expressed as (Ft – F0) /F0 as a function of time, i.e. ratio of fluorescence difference (Ft – F0) to basal value (F0). The average fluorescence intensity in the baseline period was taken as F0 and measured as the average pixel intensity during the first two to six frames of each imaging experiment. The maximum fluorescence intensity Ft was measured by calculating the average (peak – background) pixel values in a given region of interest (ROI) for each image frame recorded during the whole recording period. The Ft was then used to calculate ΔF/F using the formula $\Delta F/F = (Ft - F0)/F0$. Activation of a neuron was defined as an increase in fluorescence intensity $\Delta F/F \geq 20\%$.

Second in vivo calcium imaging system.—A different in vivo calcium imaging was also performed. The method was similar to that described above, except: Bilateral L4 and L3 DRG transverse processes and spinous processes were removed so that DRGs on both sides could be imaged. The exposed DRGs and spinal cord were rinsed with warmed (37°C) and oxygenated ACSF to remove blood and covered with a thin layer of warmed (37°C) light mineral oil. The dura remained in place. Imaging was performed for 2 – 4 hours. The spinal column was stabilized using a pair of custom-designed glass hooks to minimize movements caused by breathing and heart beats. The microscope used was a fluorescence microscope (Olympus BX-UCB microscope system), which was equipped with a fast EM-CCD camera. Live images were acquired in timelapse mode at typically 1.67 Hz at depths below the dura ranging from 0 to 10 μm for about 15 min, using a 4× /0.16 UPlanSApo dry objective at excitation 488 nm wavelength and emission at 500–549 nm for green fluorescence. Unlike the microscope in the Johns Hopkins lab, this was not a confocal microscope and only DRG neurons in the focal plane were analyzed. Hence direct comparison of cluster sizes between the two labs was not done. Raw images were collected and analyzed via Slidebook. The contrast was adjusted and selected optical planes or z projections of sequential optical sections were used to obtain final images and to produce time-lapse movies. Data using this

imaging is presented only in figures 3H-J and movie S5; all other data used the methods described in the preceding paragraphs.

Whole L4 DRG clearing with CUBIC solution—CUBIC-1 solution was prepared as described previously (Susaki et al., 2014), which is a mixture of 25 wt% urea (Sigma-Aldrich)), 25 wt% N, N, N', N'-tetrakis (2-hydroxypropyl) ethylenediamine (Sigma-Aldrich), and 15 wt% polyethylene glycol mono-pisooctylphenyl ether/Triton X-100 (Sigma-Aldrich). Mice were deeply anesthetized with sodium pentobarbital and transcardially perfused with 50 mL 0.1 M cold PBS followed by 50 mL PBS containing 4% paraformaldehyde (PFA) (pH 7.4; 4°C). L4 DRGs were dissected from the perfused mice, post-fixed in 4% PFA on ice for 1 hour, cryoprotected in 30% sucrose in PBS at 4°C overnight, and then put into CUBIC-1 solution at room temperature for 3 days. The solution was then exchanged, and DRGs was immersed for an additional 3 to 4 days. Then DRGs were examined and images were obtained with a Zeiss 700 scanning confocal microscope.

Sympathetic fiber staining in DRG sections—Mice were first perfused with 0.1M phosphate buffer until clear fluid was seen, followed by perfusion with 4% paraformaldehyde for 5 minutes. DRG sections were cut at 30 μm on a cryostat after fixation in 4% paraformaldehyde, 0.1M Phosphate Buffer, 30% sucrose. The tyrosine hydroxylase antibody (TH) was from Pel-Freez (catalog P40101-150), diluted 1:500. For quantification of TH staining, images from multiple sections of each DRG, selected at random, were captured under an Olympus BX63 fluorescent microscope using Cellsens Dimension imaging software (Olympus). TH-positive fibers were traced and the total fiber length was normalized by the area measured. Only cellular areas of the DRG were quantified, and the small TH-positive sensory neurons and TH-positive fibers in the spinal nerve were not included. All image capture and analysis sessions were performed comparing samples from all experimental groups, prepared with the same staining solutions, then measured using identical display parameters. In separate experiments, tdT was used rather than TH staining to mark the sympathetic fibers. The procedure of section staining of blood vessel markers (purified rat antimouse CD31, BD Biosciences, 1:50) with sympathetic fibers (tDT signal) in Phox2bcre;tdt; PirtGFP mice was the same as described for anti-TH staining. Only tdT-positive fibers (not overlapping with CD31) in cellular areas were quantified.

Quantitative reverse transcription PCR—Total RNA was isolated from homogenized DRG using the RNeasy Plus Micro Kit (Qiagen) according to the manufacturer's recommendation. Genomic DNA was removed by using gDNA column eliminator and digesting with RNase-free DNase (Qiagen). Reverse transcription was carried out using the iScript cDNA synthesis kit (BioRad) and no-RT controls (in which the reverse transcriptase enzyme was replaced with water) were made concurrently. Gene expression was assessed utilizing pre-designed TaqMan probes (Applied Biosystems) and analyzed using a StepOnePlus real-time PCR system (Applied Biosystems). Target gene expression levels were normalized to Actb internal control and their relative expression ratios were reported as $2^{-\Delta\Delta Ct}$.

Intra-DRG microinjection with CTB—The in vivo intra-DRG microinjection was performed as previously described with minor adjustments (Hur and Zhou, 2011). Briefly, under anesthesia, a small dorsolateral laminectomy was performed on the right side to expose the right L4 DRG of a mouse. Alexa Fluor 555-conjugated cholera toxin subunit B (2 μg/μl in PBS) was slowly injected into the L4 DRG using a glass micropipette (made from a glass capillary using a pipette puller) connected to a Picospritzer III (20-psi pressure, 6-ms duration, Parker Hannifin). The wound was then closed with sutures or tissue glue.

Intra-skin and muscle microinjection with CTB—Experiments testing the origin of cluster firing neurons used the CCI model. (The SNI model was not used because the CTB555 signal was weak if we injected into the skin and muscle 3 days before injury and then waited until day 20 post-SNI to image cluster firing). At day 0, we established the CCI model. On day 18, we injected CTB 555 (2 μg/μl in PBS) into both hairy and glabrous skin in the right hind paw, and muscle in the paw and leg separately in different mice. Imaging was performed 3 days after the CTB injection.

Drug administration—Adenosine 5′-triphosphate (ATP) disodium (Sigma-Aldrich), 6-hydroxydopamine (6-OHDA) (Sigma-Aldrich), phentolamine (Sigma-Aldrich), propranolol (Sigma-Aldrich) and atipamezole (Sigma-Aldrich) were dissolved in saline. Fresh solutions were made in every experiment. Doxazosin (Sigma-Aldrich) and CNO (Sigma-Aldrich) were dissolved in 0.1% DMSO in saline. Dopamine hydrochloride (Sigma-Aldrich) and noradrenaline bitartrate (Tocris) were dissolved in saline. Drugs were applied locally to the DRG in vivo by directly dropping them onto the surface to incubate for the indicated times. At the end of the incubation period, the drug solution was replaced by a fresh 5 to 10μl drug aliquot that remained in place during the subsequent recording. Before administration of drugs and at the end of each experiment, the viability of the DRG was confirmed by observing large numbers of cells giving a calcium transient in response to brushing and pinching of the hindpaw (Figure S1G-S1H, Figure S4G-S4H, Figure S5D and S5I, Figure S7B-S7D, S7L-S7M, S7T-S7U). For intrathecal administration, drugs were injected at the position of L6 with 5μL. Administration of drugs to the DRG ensured a local site of action in imaging experiments. For intrathecal administration, the spinal cord was another possible site of action. This caveat is noted in experiments with 6-OHDA; for experiments in which Phox2B-cre was used to drive expression of chemogenetic receptors, we relied on the lack of expression in spinal cord ((Zeisel et al., 2018), and as confirmed in our lab) to ensure that the sympathetic fibers in the DRG were the site of action for CNO. Phox2b can also drive expression in the parasympathetic and enteric peripheral ganglia, but these do not send fibers into the DRG.

Intrathecal administration of AAV9—Mice were anesthetized with 1.5%–2% isoflurane gas, and maintained at around 37°C using a heating pad. An incision was made in the skin over the lumbar region and the intervertebral membrane was exposed between L2 and L1 vertebrae, the region surrounding the lumbar enlargement. A small cut was made in the membrane and the underlying dura to insert a small catheter of 0.2-mm diameter in the caudal direction, through which 5 μL of AAV9 ($1.1X10^{13}$ gc/ml) was infused into the intrathecal space. The incision was closed. AAV9-CAG-GCaMP6s was purchased from

Addgene. Custom AAV9-CAG-NE2h and Custom AAV9-CAG-DA4.4 were purchased from Vigene.

QUANTIFICATION AND STATISTICAL ANALYSIS

All applicable tests were performed and analyzed with the experimenter blind to genotype or drug. Data in figures represent mean ± standard error of the mean (SEM). Data from independent experiments were pooled when possible or represent at least two independent replicates. All significance tests were chosen considering the design of experiments, and we assumed normal distribution and variance of data. Sample sizes were chosen based upon pilot experiments in order to accurately detect statistical significance as well as considering technical feasibility, resource availability, and ethical animal and sample use. No data were excluded from statistical analyses, unless due to technical errors. Statistical significance was determined by two-tailed unpaired or paired Student's t test with Welch's correction, or by one-way ANOVA for experiments with more than two experimental groups. For experiments in which time points were compared, two-way repeated measure ANOVA with Sidak's posttest was used. In all graphs of results of parameters before and after addition of drug, the significance symbols are presented for the posttest comparison of before and after drug or vehicle application within each experimental group; in all such data the overall effect of drug * time interaction was also significant. Values <0.05 were considered significant. Further statistical details of experiments can be found in the figure legends. Statistical analyses were performed using Prism 8 or 9 (GraphPad Software). Significance is labeled as: ****$p < 0.0001$, ***$p < 0.001$, **$p < 0.01$, *$p < 0.05$, N.S., Not Significant.

Supplementary Material

Refer to Web version on PubMed Central for supplementary material.

ACKNOWLEDGEMENT

We thank Dr. Yulong Li for a genetically encoded GPCR activation-based norepinephrine (GRAB NE) and Dopamine (GRAB DA) sensors.

Funding:

This work was supported by NIH (1RF1NS113883-01 to XZ.D. and J.-M. Z., NS045594 to J.-M. Z, and K99EY031742 to X. W.). XZ.D. is an investigator at Howard Hughes Medical Institute.

REFERENCES

Baron R (2009). Neuropathic pain: a clinical perspective. Sens. Nerves 3–30.

Bennett GJ (2012). What is spontaneous pain and who has it? J. Pain 13, 921–929. [PubMed: 22824584]

Benzon H, Raja SN, Fishman SE, Liu SS, and Cohen SP (2011). Essentials of pain medicine E-book (Elsevier Health Sciences).

Brumovsky P, Villar MJ, and Hökfelt T (2006). Tyrosine hydroxylase is expressed in a subpopulation of small dorsal root ganglion neurons in the adult mouse. Exp. Neurol 200, 153–165. [PubMed: 16516890]

Charles AC, Kodali SK, and Tyndale RF (1996). Intercellular calcium waves in neurons. Mol. Cell. Neurosci 7, 337–353. [PubMed: 8812061]

Chen T-W, Wardill TJ, Sun Y, Pulver SR, Renninger SL, Baohan A, Schreiter ER, Kerr RA, Orger MB, and Jayaraman V (2013). Ultrasensitive fluorescent proteins for imaging neuronal activity. Nature 499, 295–300. [PubMed: 23868258]

Chisholm KI, Khovanov N, Lopes DM, La Russa F, and McMahon SB (2018). Large scale in vivo recording of sensory neuron activity with GCaMP6. Eneuro 5.

Cho H-J, Kim D-S, Lee N-H, Kim J.-k., Lee K-M, Han K-S, Kang Y-N, and Kim K-J (1997). Changes in the α2-adrenergic receptor subtypes gene expression in rat dorsal root ganglion in an experimental model of neuropathic pain. Neuroreport 8, 3119–3122. [PubMed: 9331925]

Dahlhamer J, Lucas J, Zelaya C, Nahin R, Mackey S, DeBar L, Kerns R, Von Korff M, Porter L, and Helmick C (2018). Prevalence of chronic pain and high-impact chronic pain among adults—United States, 2016. Morb. Mortal. Wkly. Rep 67, 1001.

Devor M (2009). Ectopic discharge in Aβ afferents as a source of neuropathic pain. Exp. Brain Res 196, 115–128. [PubMed: 19242687]

Djouhri L, Koutsikou S, Fang X, McMullan S, and Lawson SN (2006). Spontaneous pain, both neuropathic and inflammatory, is related to frequency of spontaneous firing in intact C-fiber nociceptors. J. Neurosci 26, 1281–1292. [PubMed: 16436616]

Du W-J, Hu S, Li X, Zhang P-A, Jiang X, Yu S-P, and Xu G-Y (2019). Neonatal maternal deprivation followed by adult stress enhances adrenergic signaling to advance visceral hypersensitivity. Neurosci. Bull 35, 4–14. [PubMed: 30560437]

Dubuisson D, and Dennis SG (1977). The formalin test: A quantitative study of the analgesic effects of morphine, meperidine, and brain stem stimulation in rats and cats. Pain 4, 161–174. [PubMed: 564014]

Emery EC, Luiz AP, Sikandar S, Magnúsdóttir R, Dong X, and Wood JN (2016). In vivo characterization of distinct modality-specific subsets of somatosensory neurons using GCaMP. Sci. Adv 2, e1600990. [PubMed: 27847865]

Feng J, Zhang C, Lischinsky JE, Jing M, Zhou J, Wang H, Zhang Y, Dong A, Wu Z, and Wu H (2019). A genetically encoded fluorescent sensor for rapid and specific in vivo detection of norepinephrine. Neuron 102, 745–761. [PubMed: 30922875]

Furlan A, La Manno G, Lübke M, Häring M, Abdo H, Hochgerner H, Kupari J, Usoskin D, Airaksinen MS, and Oliver G (2016). Visceral motor neuron diversity delineates a cellular basis for nipple-and pilo-erection muscle control. Nat. Neurosci 19, 1331–1340. [PubMed: 27571008]

Guan Y, Liu Q, Tang Z, Raja SN, Anderson DJ, and Dong X (2010). Mas-related G-protein-coupled receptors inhibit pathological pain in mice. Proc. Natl. Acad. Sci. U. S. A 107, 15933–15938. [PubMed: 20724664]

Gyires K, Zádori ZS, Török T, and Mátyus P (2009). α2-Adrenoceptor subtypes-mediated physiological, pharmacological actions. Neurochem. Int 55, 447–453. [PubMed: 19477210]

Han DW, Kweon TD, Kim KJ, Lee JS, Chang CH, and Lee Y-W (2006). Does the tibial and sural nerve transection model represent sympathetically independent pain? Yonsei Med. J 47, 847–851. [PubMed: 17191315]

Huang L, Ledochowitsch P, Knoblich U, Lecoq J, Murphy GJ, Reid RC, de Vries SEJ, Koch C, Zeng H, and Buice MA (2021). Relationship between simultaneously recorded spiking activity and fluorescence signal in GCaMP6 transgenic mice. Elife 10, e51675. [PubMed: 33683198]

Huber K (2006). Cholinergic differentiation occurs early in mouse sympathetic neurons and requires Phox2b. Gene Expr. J. Liver Res 13, 133–139.

Hur E-M, and Zhou F-Q (2011). Genetic dissection of axon regeneration via in vivo electroporation of adult mouse sensory neurons. Nat. Commun 2, 1–10.

Jänig W (2014). Sympathetic nervous system and inflammation: a conceptual view. Auton. Neurosci 182, 4–14. [PubMed: 24525016]

Jourdan D, Ardid D, Bardin L, Bardin M, Neuzeret D, Lanphouthacoul L, and Eschalier A (1997). A new automated method of pain scoring in the formalin test in rats. Pain 71, 265–270. [PubMed: 9231869]

Kajander KC, Wakisaka S, and Bennett GJ (1992). Spontaneous discharge originates in the dorsal root ganglion at the onset of a painful peripheral neuropathy in the rat. Neurosci. Lett 138, 225–228. [PubMed: 1319012]

Kim AY, Tang Z, Liu Q, Patel KN, Maag D, Geng Y, and Dong X (2008). Pirt, a phosphoinositide-binding protein, functions as a regulatory subunit of TRPV1. Cell 133, 475–485. [PubMed: 18455988]

Kim YS, Anderson M, Park K, Zheng Q, Agarwal A, Gong C, Young L, He S, LaVinka PC, and Zhou F (2016). Coupled activation of primary sensory neurons contributes to chronic pain. Neuron 91, 1085–1096. [PubMed: 27568517]

Kuchibhotla KV, Lattarulo CR, Hyman BT, and Bacskai BJ (2009). Synchronous hyperactivity and intercellular calcium waves in astrocytes in Alzheimer mice. Science (80-.). 323, 1211–1215.

Light KC, Bragdon EE, Grewen KM, Brownley KA, Girdler SS, and Maixner W (2009). Adrenergic dysregulation and pain with and without acute beta-blockade in women with fibromyalgia and temporomandibular disorder. J. Pain 10, 542–552. [PubMed: 19411061]

Ma W, Zhang Y, Bantel C, and Eisenach JC (2005). Medium and large injured dorsal root ganglion cells increase TRPV-1, accompanied by increased α2C-adrenoceptor co-expression and functional inhibition by clonidine. Pain 113, 386–394. [PubMed: 15661448]

Maruo K, Yamamoto H, Yamamoto S, Nagata T, Fujikawa H, Kanno T, Yaguchi T, Maruo S, Yoshiya S, and Nishizaki T (2006). Modulation of P2X receptors via adrenergic pathways in rat dorsal root ganglion neurons after sciatic nerve injury. Pain 120, 106–112. [PubMed: 16360272]

Mazzuca M, and Poulain P (1974). Ultrastructural identification of monoamine-containing nerve endings in the guinea-pig median eminence (author's transl). Brain Res. 68, 281–295. [PubMed: 4151197]

McCorry LK (2007). Physiology of the autonomic nervous system. Am. J. Pharm. Educ 71.

McLachlan EM, Jänig W, Devor M, and Michaelis M (1993). Peripheral nerve injury triggers noradrenergic sprouting within dorsal root ganglia. Nature 363, 543–546. [PubMed: 8505981]

Mogil JS (2009). Animal models of pain: progress and challenges. Nat. Rev. Neurosci 10, 283–294. [PubMed: 19259101]

Mogil JS (2012). The etiology and symptomatology of spontaneous pain. J. Pain 13, 932–933. [PubMed: 23031393]

Murai N, Sekizawa T, Gotoh T, Watabiki T, Takahashi M, Kakimoto S, Takahashi Y, Iino M, and Nagakura Y (2016). Spontaneous and evoked pain-associated behaviors in a rat model of neuropathic pain respond differently to drugs with different mechanisms of action. Pharmacol. Biochem. Behav 141, 10–17. [PubMed: 26597514]

Odem MA, Bavencoffe AG, Cassidy RM, Lopez ER, Tian J, Dessauer CW, and Walters ET (2018). Isolated nociceptors reveal multiple specializations for generating irregular ongoing activity associated with ongoing pain. Pain 159, 2347. [PubMed: 30015712]

Pattyn A, Morin X, Cremer H, Goridis C, and Brunet J-F (1999). The homeobox gene Phox2b is essential for the development of autonomic neural crest derivatives. Nature 399, 366–370. [PubMed: 10360575]

Pertin M, Allchorne AJ, Beggah AT, Woolf CJ, and Decosterd I (2007). Delayed sympathetic dependence in the spared nerve injury (SNI) model of neuropathic pain. Mol. Pain 3, 1744–8069.

Prescott SA, and Ratté S (2012). Pain processing by spinal microcircuits: afferent combinatorics. Curr. Opin. Neurobiol 22, 631–639. [PubMed: 22409855]

Sapio M, Vazquez FA, Loydpierson AJ, Marie D, Kim JJ, LaPaglia DM, Puhl HL, Lu VB, Ikeda SR, and Mannes AJ (2020). Comparative analysis of dorsal root, nodose and sympathetic ganglia for the development of new analgesics. Front. Neurosci 14, 1332.

Schmalbruch H (1987). The number of neurons in dorsal root ganglia L4–L6 of the rat. Anat. Rec 219, 315–322. [PubMed: 3322108]

Shinder V, Govrin-Lippmann R, Cohen S, Belenky M, Ilin P, Fried K, Wilkinson HA, and Devor M (1999). Structural basis of sympathetic-sensory coupling in rat and human dorsal root ganglia following peripheral nerve injury. J. Neurocytol 28, 743–761. [PubMed: 10859576]

Sørensen B, Tandrup T, Koltzenburg M, and Jakobsen J (2003). No further loss of dorsal root ganglion cells after axotomy in p75 neurotrophin receptor knockout mice. J. Comp. Neurol 459, 242–250. [PubMed: 12655507]

Strong JA, Zhang J-M, and Schaible H-G (2018). The sympathetic nervous system and pain. In The Oxford Handbook of the Neurobiology of Pain, (Oxford University Press), pp. 1–25.

Sun F, Zeng J, Jing M, Zhou J, Feng J, Owen SF, Luo Y, Li F, Wang H, and Yamaguchi T (2018). A genetically encoded fluorescent sensor enables rapid and specific detection of dopamine in flies, fish, and mice. Cell 174, 481–496. [PubMed: 30007419]

Susaki EA, Tainaka K, Perrin D, Kishino F, Tawara T, Watanabe TM, Yokoyama C, Onoe H, Eguchi M, and Yamaguchi S (2014). Whole-brain imaging with single-cell resolution using chemical cocktails and computational analysis. Cell 157, 726–739. [PubMed: 24746791]

Tonello R, Xie W, Lee SH, Wang M, Liu X, Strong JA, Zhang J-M, and Berta T (2020). Local sympathectomy promotes anti-inflammatory responses and relief of paclitaxel-induced mechanical and cold allodynia in mice. Anesthesiology 132, 1540–1553. [PubMed: 32404819]

Truini A, Galeotti F, Haanpaa M, Zucchi R, Albanesi A, Biasiotta A, Gatti A, and Cruccu G (2008). Pathophysiology of pain in postherpetic neuralgia: a clinical and neurophysiological study. Pain 140, 405–410. [PubMed: 18954941]

Truini A, Padua L, Biasiotta A, Caliandro P, Pazzaglia C, Galeotti F, Inghilleri M, and Cruccu G (2009). Differential involvement of A-delta and A-beta fibres in neuropathic pain related to carpal tunnel syndrome. PAIN 145, 105–109. [PubMed: 19535205]

Uttam S, Wong C, Amorim IS, Jafarnejad SM, Tansley SN, Yang J, Prager-Khoutorsky M, Mogil JS, Gkogkas CG, and Khoutorsky A (2018). Translational profiling of dorsal root ganglia and spinal cord in a mouse model of neuropathic pain. Neurobiol. Pain 4, 35–44. [PubMed: 30906902]

Walters ET (2018). How is chronic pain related to sympathetic dysfunction and autonomic dysreflexia following spinal cord injury? Auton. Neurosci 209, 79–89. [PubMed: 28161248]

Wang F, Bélanger E, Côté SL, Desrosiers P, Prescott SA, Côté DC, and De Koninck Y (2018). Sensory afferents use different coding strategies for heat and cold. Cell Rep. 23, 2001–2013. [PubMed: 29768200]

Wilkins M, and Sneyd J (1998). Intercellular spiral waves of calcium. J. Theor. Biol 191, 299–308. [PubMed: 9631570]

Xie W, Strong JA, Mao J, and Zhang J-M (2011). Highly localized interactions between sensory neurons and sprouting sympathetic fibers observed in a transgenic tyrosine hydroxylase reporter mouse. Mol. Pain 7, 1744–8069.

Xie W, Chen S, Strong JA, Li A-L, Lewkowich IP, and Zhang J-M (2016). Localized sympathectomy reduces mechanical hypersensitivity by restoring normal immune homeostasis in rat models of inflammatory pain. J. Neurosci 36, 8712–8725. [PubMed: 27535916]

Xie W, Strong JA, and Zhang J-M (2020). Localized sympathectomy reduces peripheral nerve regeneration and pain behaviors in 2 rat neuropathic pain models. Pain 161, 1925–1936. [PubMed: 32701850]

Zeisel A, Hochgerner H, Lönnerberg P, Johnsson A, Memic F, Van Der Zwan J, Häring M, Braun E, Borm LE, and La Manno G (2018). Molecular architecture of the mouse nervous system. Cell 174, 999–1014. [PubMed: 30096314]

Zheng Q, Fang D, Cai J, Wan Y, Han J-S, and Xing G-G (2012). Enhanced excitability of small dorsal root ganglion neurons in rats with bone cancer pain. Mol. Pain 8, 24. [PubMed: 22472208]

HIGHLIGHTS

- Spontaneous cluster firing is a new form of DRG neuron activity after nerve injury
- Spontaneous DRG cluster firing mediates spontaneous pain after nerve injury
- Norepinephrine released from sympathetic nerves in the DRG drives cluster firing
- Blocking cluster firing effectively inhibits neuropathic spontaneous pain

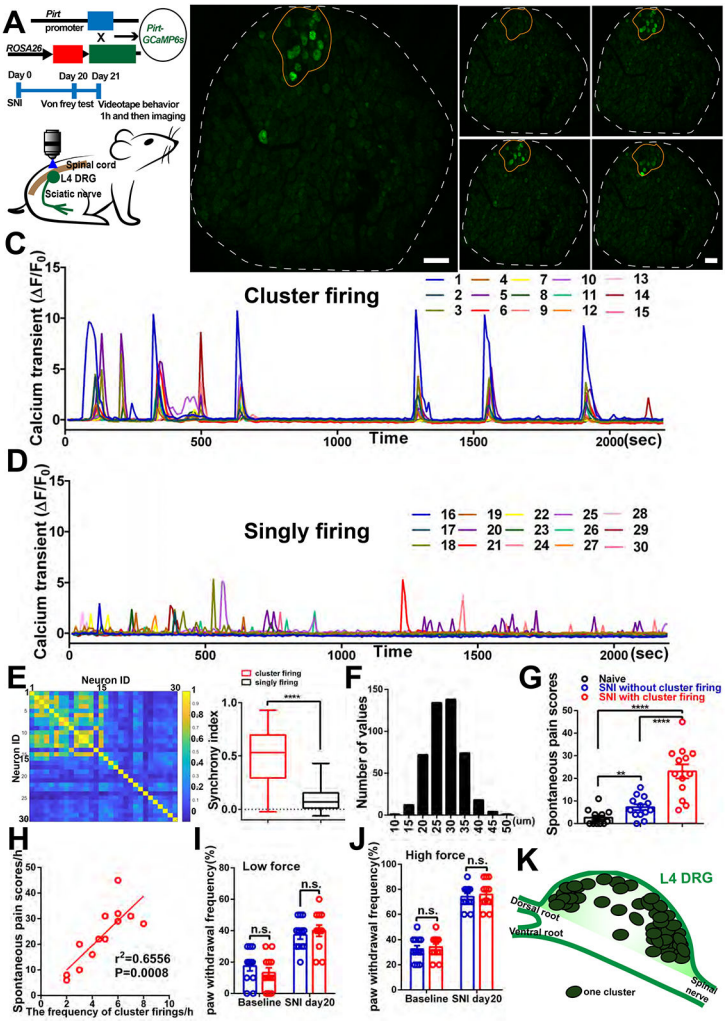

Figure 1. Spontaneous CFEs revealed by in vivo DRG calcium imaging after peripheral nerve injury.

(A) Upper: Diagram showing the mating strategy. Middle: Experimental flowchart. Lower: Schematic diagram illustrating in vivo calcium imaging.

(B) Representative images of one cluster (orange circle) observed during in vivo calcium imaging of L4 DRG (white outline indicates DRG border) in SNI mouse. Image shows neurons in the cluster firing synchronously at different times (B0– B3).

(C) Time course of calcium transients in individual neurons from the cluster in (B), in which all neurons are labeled and traced.

(D) Time course of calcium transients in 15 individual singly firing neurons scattered throughout the DRG in (B), labels not shown.

(E) Pairwise correlations of 30 neurons in (C) and (D). Left: all pairs' correlations; color bar indicates the correlations of cluster firing neurons (neuron ID 1 to 15) and singly firing neurons (neuron ID 16-30) that form the pairs. Right: pairs of cluster firing neurons show significantly stronger synchrony than pairs of singly firing neurons. The synchrony index was calculated as the average correlation. There are 15 neurons in each group, so there are 105 correlation values in each group.

(F) The distribution of diameters of clustered firing neurons, summarized from 18 mice with cluster firing data.
(G) Spontaneous pain scores in naïve mice and SNI mice (Day 21) with and without cluster firing.
(H) Pearson correlation between the frequencies of cluster firing recorded during in vivo imaging and spontaneous pain scores (from SNI mice in (G) that showed cluster firing).
(I-J) Mechanical pain induced by low force (0.07g) and high force (0.4g) von Frey filaments in SNI mice without and with cluster firing.
(K) Diagram for locations of clusters within the whole DRG summarizing 58 clusters identified in 22 SNI mice with cluster firing.
Scale bar, 100 μm. Each open circle in (G) to (J) represents an individual mouse. Data are represented as mean ± SEM. **p < 0.01; ****p < 0.0001; n.s., not significant; (E) by unpaired two-tailed t test; (G) by One-way ANOVA with Tukey's posttest; (I) and (J) by two-way repeated measures ANOVA with Sidak's posttest.

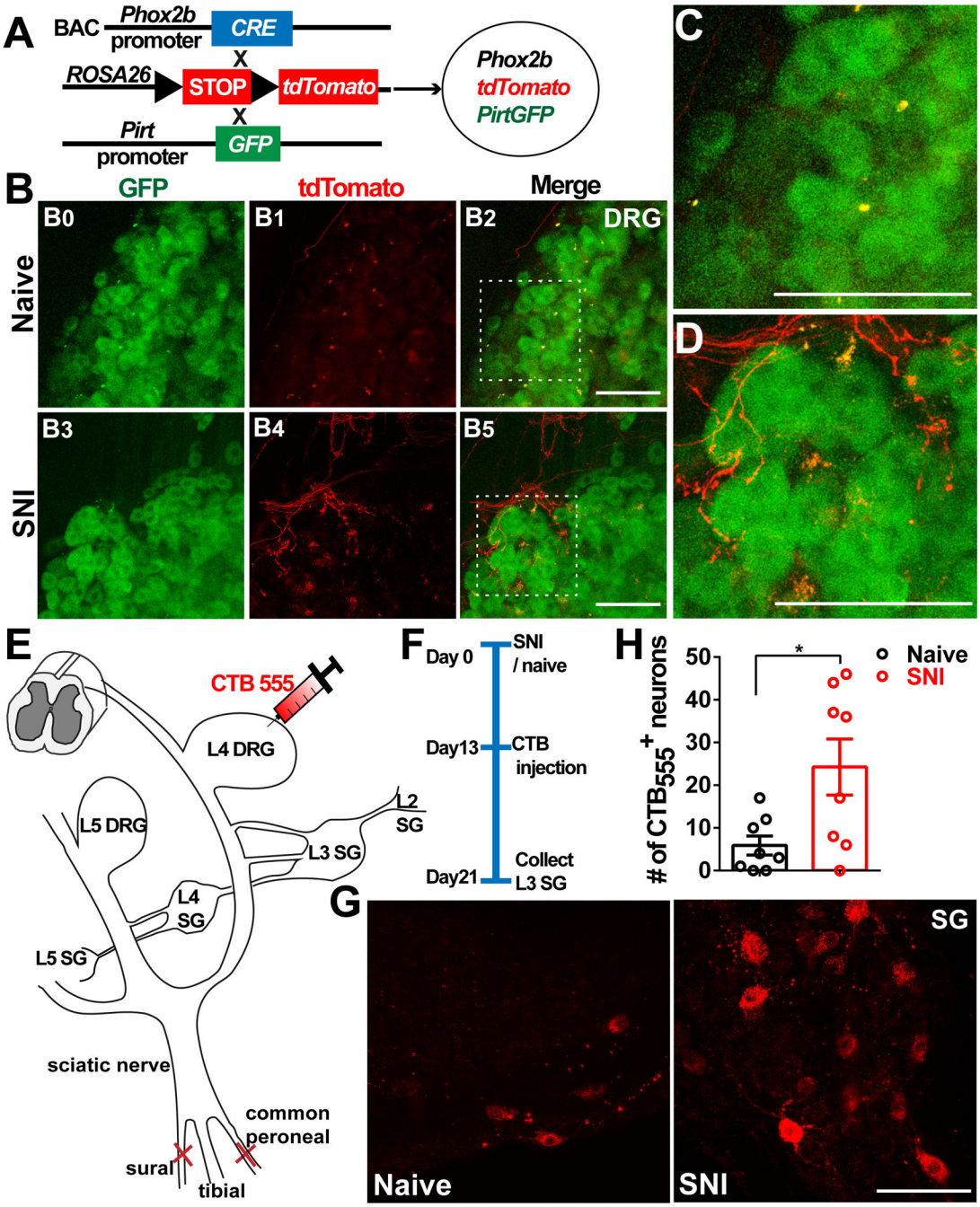

Figure 2. Sympathetic nerve fibers sprout into DRGs after peripheral nerve injury

(A) Diagram showing the mating strategy. GFP is expressed in DRG neurons, tdT is expressed in the sympathetic axons.

(B–D) Whole-mount cleared L4 DRGs of mice with and without SNI (day 21).

(B0–B2) Naive mouse.

(B3–B5) SNI mouse.

(C) Magnification of the boxed region in (B2), showing no tdT-positive fibers sprouting into the DRG.

(D) Magnification of the boxed region in (B5), showing tdT-positive fibers sprouting into the DRG.
(E) Schematic of retrograde CTB tracing in a sympathetic ganglion. The red needle indicates the position of CTB555 injection.
(F) The experimental procedure: SNI surgery on day 0, injection of CTB555 into L4 DRGs on day 13, and dissection of L3 sympathetic ganglia on day 21.
(G) Representative images of L3 sympathetic ganglia of naive and SNI mice.
(H) Summary data of the number of CTB-positive neurons in the L3 sympathetic ganglion. Scale bars, 100 um. Each open circle represents an individual mouse. Data are presented as mean ± SEM. *$p < 0.05$; (H) by two-tailed unpaired t test.

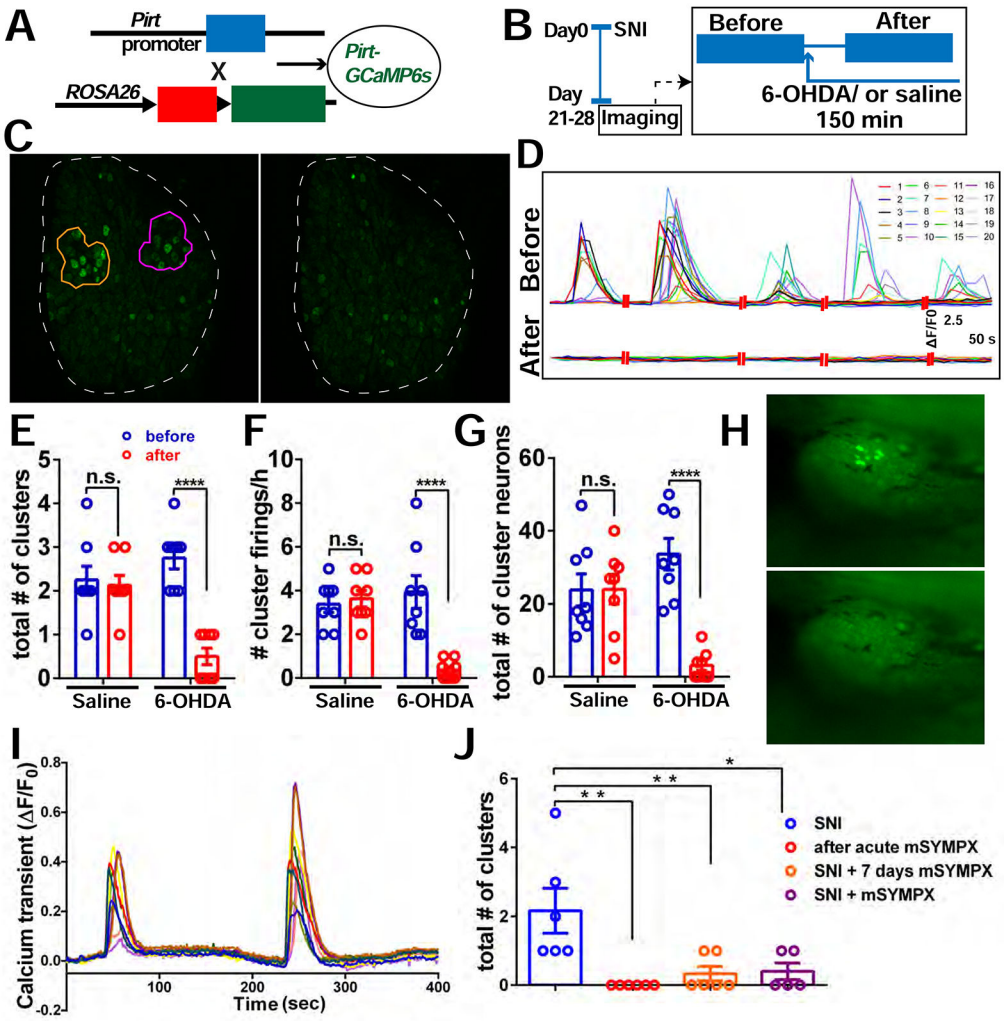

Figure 3. Pharmacological inhibition of sympathetic nerve activity in the DRG and mSYMPX reduce incidence of CFEs.

(A) Diagram showing the mating strategy. *Pirt-Cre; GCaMP6s* mice were used.

(B) Experimental schematic. We first imaged the mice with SNI at POD 21-28 for 2 hours. If CFEs were observed, 0.5 mM 6-OHDA solution was then applied topically onto the DRG and allowed to incubate for 30 minutes, followed by an additional 2 hours of recording with about 5 to 10 μL 6-OHDA solution covering the DRG.

(C) An example of cluster firing that decreased after 6-OHDA application. Left is before using 6-OHDA, and there are 2 clusters (orange and purple circle).

(D) Representative traces of individual neurons in the orange cluster which are numbered in (C) before and after addition of 6-OHDA.

(E-G) The total number of clusters (E), frequency of cluster firing (F), and total number of cluster firing neurons (G) significantly decreased after addition of 6-OHDA to DRG but not after addition of saline.

(H) An example of a cluster firing event in the L4 DRG, 4 weeks after SNI. Before (upper) and after (lower) localized microsympathectomy (mSYMPX).

(I) Representative traces of individual neurons in (H) before mSYMPX.

(J) The number of CFEs was reduced by mSYMPX, whether performed acutely during the recording, at the time of SNI, or 7 days prior to recording after the SNI model had been established for 4 weeks.

Scale bar, 100 μm (C); 250 μm (H). Each pair of open circles (before and after) represents an individual mouse. Data are represented as mean ± SEM. **p < 0.01; ****p < 0.0001; n.s., not significant; (E) to (G) by two-way repeated measures ANOVA with Sidak's posttest, (J) by oneway ANOVA with Dunnett's posttest.

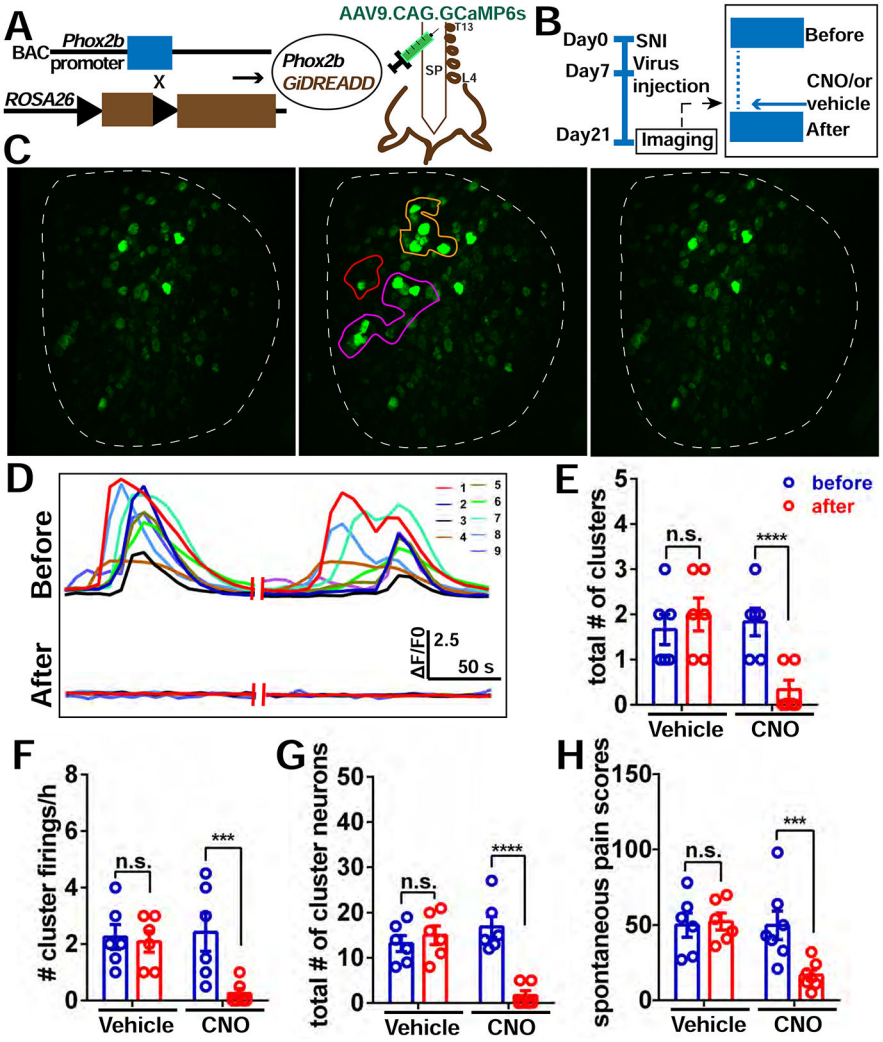

Figure 4. Chemogenetic silencing of sympathetic nerve activity in the DRG diminishes the incidence of CFEs and relieves spontaneous pain.

(A) Diagram showing the mating strategy and intrathecal injection with AAV9.CAG.GCaMP6s in *Phox2bCre; GiDREADD* mice.

(B) Diagram showing the experimental procedure. On POD 21, in vivo imaging of L4 DRG was first recorded for 2 hours followed by topical application of 10 μM CNO or vehicle (0.1%DMSO) on the surface of the DRG to locally activate the DREADD receptors in sympathetic nerves. In vivo imaging was then resumed for an additional 2 hours.

(C) An example of decreased cluster firing after local addition of CNO on the DRG. Left is quiescent (i.e. period with no cluster firing); Middle is an example of cluster firing before CNO addition. There are 3 clusters (orange, purple and red circles). Right is after CNO addition, all 3 clusters were diminished.

(D) Representative traces of neurons in the orange cluster which are numbered in (C) before and after administration of CNO.

(E-G) The total number of clusters (E), frequency of cluster firing (F), and total number of cluster firing neurons (G) is significantly inhibited after addition of CNO to DRG, but not with addition of vehicle (0.1% DMSO in saline).

(H) Spontaneous pain scores significantly decreased after i.t. administration of CNO in SNI mice (Day 20) with cluster firing. No change was observed with administration of vehicle. Scale bar, 100 μm. Each pair of open circles (before and after) represents an individual mouse. Data are represented as mean ± SEM. ***$p < 0.001$; ****$p < 0.0001$; n.s., not significant; (E) to (H) by two-way repeated measures ANOVA with Sidak's posttest.

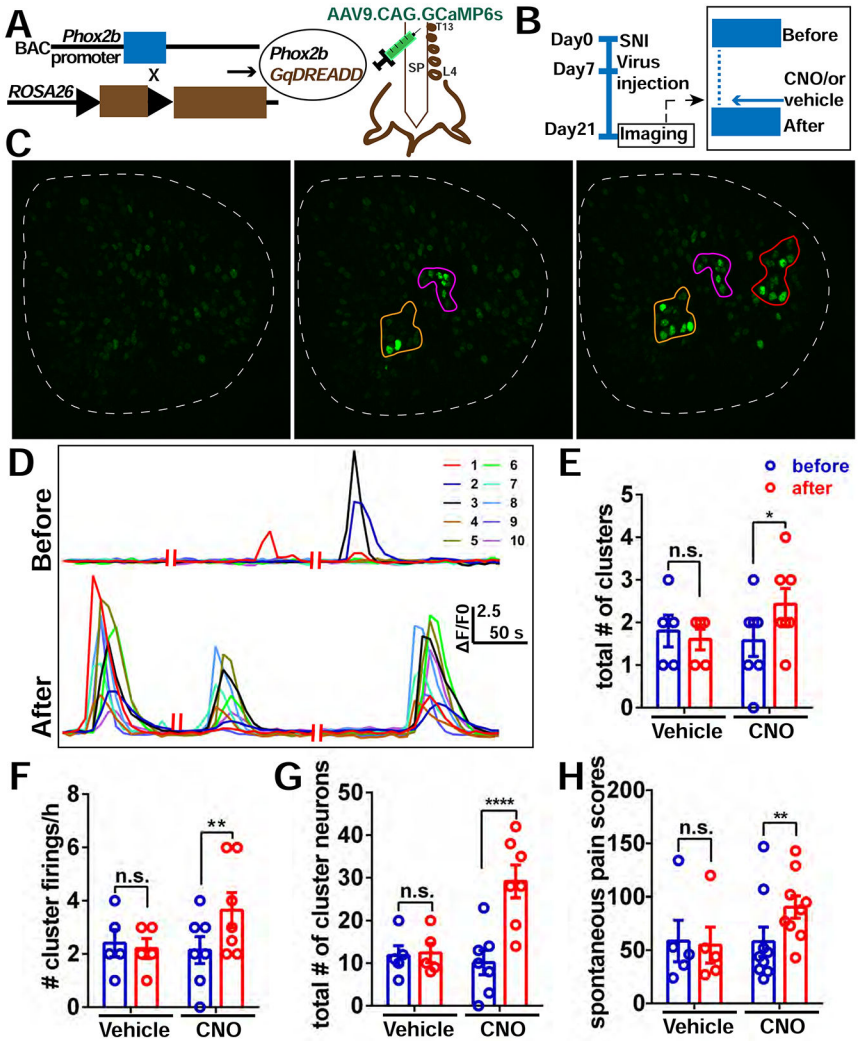

Figure 5. Chemogenetic activation of sympathetic nerve activity in the DRG enhances the incidence of CFEs and spontaneous Pain.

(A) Diagram showing the mating strategy and intrathecal injection with AAV9.CAG.GCaMP6s in *Phox2bCre; GqDREADD* mice.

(B) Diagram showing the experimental procedure. The details are the same as described in Figure 4B.

(C) An example of increased cluster firing after local addition of CNO on DRG. Left is quiescent; Middle is an example of cluster firing before addition of CNO. There are 2 clusters (orange and purple circles); Right is after addition of CNO, and there are 3 clusters (orange, purple and red circles).

(D) Representative traces of neurons in the orange cluster which are numbered in (c) before and after administration of CNO.

(E-G) The total number of clusters (E), frequency of cluster firing (F), and total number of cluster firing neurons (G) significantly increased after addition of CNO but not vehicle to the DRG.

(H) Spontaneous pain scores significantly increased after i.t. administration of CNO to SNI mice (Day 20) with cluster firing, but not after administration of vehicle.

Scale bar, 100 μm. Each pair of open circles (before and after) represents an individual mouse. Data are represented as mean ± SEM. *p < 0.05; **p < 0.01; ****p < 0.0001; n.s., not significant;(E) to (H) by two-way repeated measures ANOVA with Sidak's posttest.

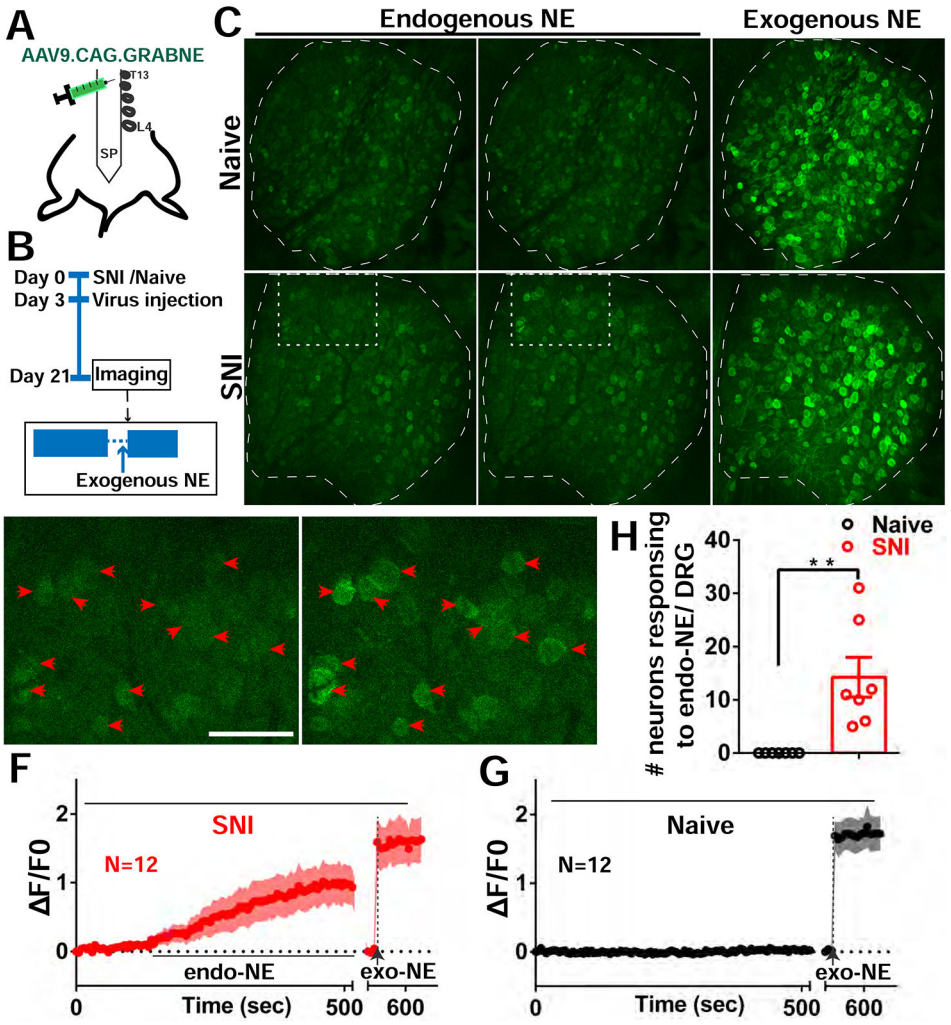

Figure 6. Endogenous NE release in DRGs after SNI.

(A) Diagram showing the i.t. injection with AAV9.CAG.GRABNE in WT mice.

(B) Diagram showing the experimental procedure.

(C) Representative images of NE sensor signals of naive and SNI mice. Naive mice had no endogenous NE released. Mice with SNI show endogenous NE released sporadically (white rectangle). At the end of the recording session exogenous NE is dropped onto DRG (both naive and SNI mice showed NE sensor activation).

(D-E) Enlarged image of rectangle area from SNI image in (C). Red arrowheads indicate 12 neurons with spontaneous NE signals (cluster activation) from quiescent (D) and release periods (E).

(F-G) Averaged NE signal traces with ±95% confidence intervals for the 12 neurons indicated by arrowheads in SNI mouse (F) and 12 randomly selected neurons from naive mouse (G).

(H) Summary of NE sensor imaging from SNI and Naive mice. DRG of SNI mice exhibit a significantly higher number of neurons responding to endogenous NE release.

Scale bar, 100 μm. Each open circle represents an individual mouse. Data are represented as mean ± SEM. **$p < 0.01$; (H) by two-tailed unpaired t test.

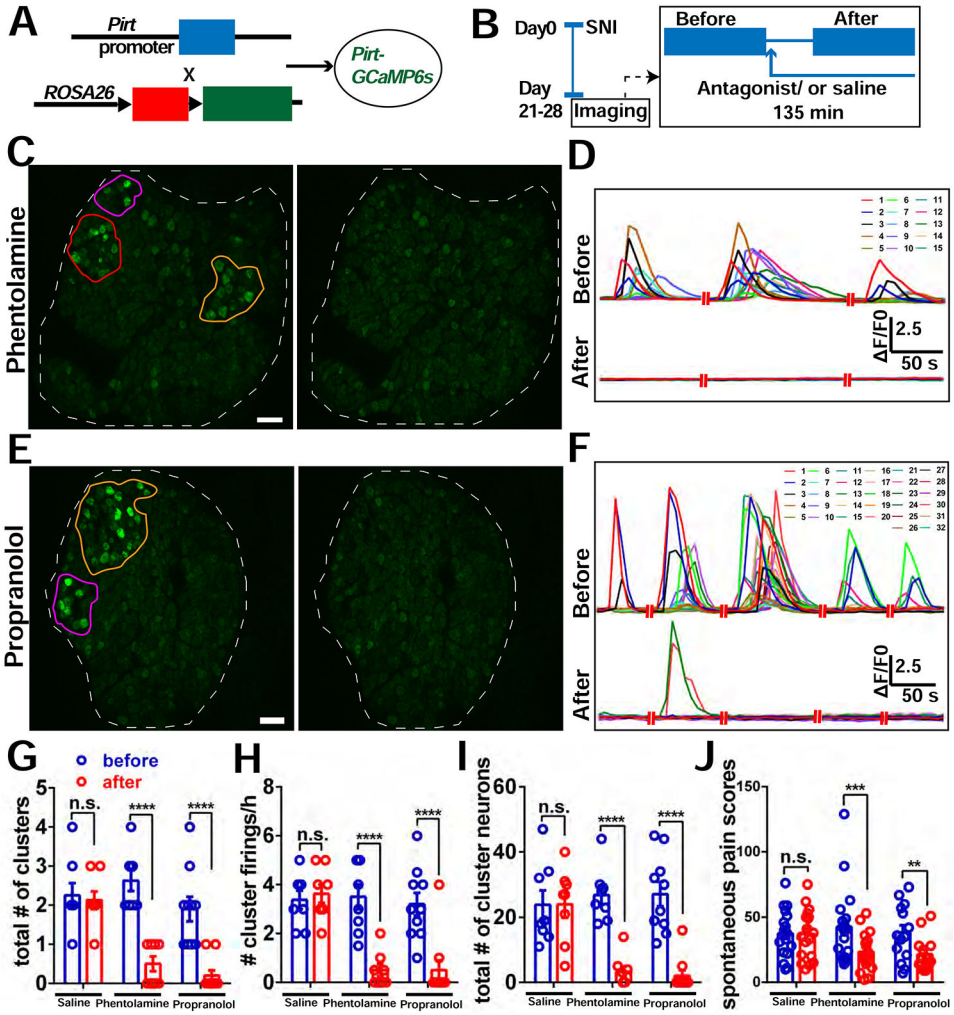

Figure 7. Block of adrenergic receptors in DRG reduces incidence of CFEs and relieves spontaneous pain.

(A) Diagram showing the mating strategy.

(B) Diagram showing the experimental procedure. We imaged the *Pirt-GCaMP6* mice with SNI at POD 21-28 for 2 hours. If CFEs were observed, a sympathetic blocker, either phentolamine (5 μM), or propranolol (1 μM) or vehicle (saline) solution was then applied topically onto the DRG and allowed to incubate for 15 minutes, followed by an additional 2 hours of recording with about 5 to 10 μL solution covering the DRG.

(C) An example of cluster firing that decreased after using phentolamine (antagonist of α-receptor). There are 3 clusters (orange, purple and red circles) before addition of phentolamine. All clusters are inhibited after.

(D) Representative traces of neurons in the orange cluster which are numbered in (C) before and after addition of phentolamine.

(E) An example of cluster firing that decreased after using propranolol (antagonist of β-receptor). There are 2 clusters (orange and purple circles) before addition of propranolol. Both clusters are inhibited after.

(F) Representative traces of neurons in the orange cluster which are numbered in (E) before and after addition of propranolol.

(G-I) The total number of clusters (G), frequency of cluster firing (H), and total number of cluster firing neurons (I) significantly decreased after addition of antagonists of adrenergic receptors on DRG, but not with addition of saline. The data of the saline group are the same as in Fig. 2.

(J) Spontaneous pain scores significantly decreased after i.t. administration of either 5μL, 10μM phentolamine or 5μL, 10μM propranolol, or 5μL vehicle alone to SNI mice, but not after administration of vehicle.

Scale bar, 100 μm. Each pair of open circles (before and after) represents an individual mouse. Data are represented as mean ± SEM. **p < 0.01; ***p < 0.001; ****p < 0.0001; n.s., not significant; (G) to (J) by two-way repeated measures ANOVA with Sidak's posttest.

Key resources table

REAGENT or RESOURCE	SOURCE	IDENTIFIER
Antibodies		
Anti-tyrosine hydroxylase antibody	Pel-Freeze	Cat# P40101 RRID: AB_2617184
Anti-CD31 antibody	BD-Biosciences	Cat# 550274 RRID: AB_393571
Goat anti-Rat Secondary Antibody, Alexa Fluor 647	Invitrogen/Thermo Fisher	Cat# A21247 RRID: AB_141778
Bacterial and virus strains		
AAV9-CAG-GCaMP6s	Addgene (Chen, et al.,2013)	pAAV.CAG.GCaMP6s.WPRE.SV40 Catalog # 100844-AAV9
Custom AAV9-CAG-NE2h	Vigene Biosciences	N/A
Custom AAV9-CAG-DA4.4	Vigene Biosciences	N/A
Biological samples		
Chemicals, peptides, and recombinant proteins		
6-Hydroxydopamine hydrochloride	Sigma-Aldrich	Cat# H4381-100MG
Phentolamine hydrochloride	Sigma-Aldrich	Cat# P7547-100MG
(±)-Propranolol hydrochloride	Sigma-Aldrich	Cat# P0884-1G
Doxazosin mesylate	Sigma-Aldrich	Cat# D9815-50MG
Lidocaine HCl	Vetone	Cat# 510213
Atipamezole	Sigma-Aldrich	Cat# A9611
Carbenoxolone disodium salt	Sigma-Aldrich	Cat# C4790-1G
Clozapine N-oxide	Sigma-Aldrich	Cat# C0832-5MG
Dopamine hydrochloride	Sigma-Aldrich	Cat# H8502-25G
Noradrenaline bitartrate	Tocris	Cat# 5169
Cholera toxin subunit B, Alexa Fluor™ 555 Conjugate	Invitrogen	Cat# C22843
Urea	Sigma-Aldrich	Cat# U5378-1KG
N,N,N',N'-Tetrakis(2-Hydroxypropyl)ethylenediamin	Sigma-Aldrich	Cat# 122262-1L
Triton X-100	Sigma-Aldrich	Cat# T9284-100ML
Adenosine 5′-triphosphate (ATP) disodium	Sigma-Aldrich	Cat# A1852-30MG
Paraformaldehyde Solution, 4% in PBS	Thermo Scientific	Cat# AAJ19943K2
DMEM	Gibco	Cat# 11995065
Fetal calf serum	Gibco	Cat# 26140079
Critical commercial assays		
RNeasy Plus Micro Kit	Qiagen	Cat# 74034
RNase-free DNase	Qiagen	Cat# 79256
iScript cDNA synthesis kit	Bio-Rad	Cat# 1708891BUN
Deposited data		
Experimental models: Cell lines		

REAGENT or RESOURCE	SOURCE	IDENTIFIER
B16F10 melanoma cells	ATCC	Cat# ATCC® CRL-6475™
Experimental models: Organisms/strains		
Mouse: C57BL/6 mice	Jackson Laboratories	Cat# JAX:000664 RRID: IMSR_JAX:000664
Mouse: *Phox2b-Cre*	Jackson Laboratories	Cat# JAX: 016223 RRID:IMSR_JAX:016223
Mouse: *GFAP-Cre*	Jackson Laboratories	Cat# JAX: 012886 RRID:IMSR_JAX:012886
Mouse: Ai14 strain B6.*Rosa26-stop (flox)-tdTomato*	Jackson Laboratories	Cat# JAX: 007914 RRID:IMSR_JAX:007914
Mouse: *Rosa26-LSL-hM3Dq-DREADD*	Jackson Laboratories	Cat# JAX: 026220 RRID:IMSR_JAX:026220
Mouse: Rosa26-LSL-hM4Di-DREADD	Jackson Laboratories	Cat# JAX: 026219 RRID:IMSR_JAX:026219
Mouse: *Pirt-Cre*	This lab (Kim et al., 2016)	N/A
Mouse: *Pirt-GCaMP3 (GFP)*	This lab (Kim et al., 2008)	N/A
Mouse: *Rosa26-LSL-GCaMP6s*	Bergles Lab at JHU	N/A
Oligonucleotides		
Assay ID:Mm00442668_m1 ; Gene Symbol: Adra1a	Applied Biosystems	Cat# 4331182
Assay ID:Mm00431685_m1 ; Gene Symbol:Adra1b	Applied Biosystems	Cat# 4331182
Assay ID:Mm01328600_m1 ; Gene Symbol:Adra1d	Applied Biosystems	Cat# 4331182
Assay ID:Mm07295458_s1; Gene Symbol:Adra2a	Applied Biosystems	Cat# 4331182
Assay ID:Mm00477390_s1 Gene Symbol:Adra2b	Applied Biosystems	Cat# 4331182
Assay ID:Mm00431686_s1 ; Gene Symbol:Adra2c	Applied Biosystems	Cat# 4331182
Assay ID:Mm00431701_s1; Gene Symbol:Adrb1	Applied Biosystems	Cat# 4331182
Assay ID:Mm02524224_s1 Gene Symbol:Adrb2	Applied Biosystems	Cat# 4331182
Assay ID:Mm02601819_g1 Gene Symbol:Adrb3	Applied Biosystems	Cat# 4331182
Assay ID:Mm01205647_g1 Gene Symbol:Actb	Applied Biosystems	Cat# 4331182
RecombinantDNA		
Software and algorithms		
FIJI	NIH	RRID: SCR_003070
Prism 8, 9	GraphPad Software	N/A
Cellsens Dimension imaging software	Olympus	N/A
Other		
Confocal microscope	Leica	TCS LSI
Fluorescent microscope	Olympus	BX63
StepOnePlus real-time PCR system	Applied Biosystems	4376598